

### КРАТКИЕ СООБЩЕНИЯ ОИЯИ

### JINR RAPID COMMUNICATIONS

2[70]-95

JINR Informational and Computing Framework Development	
The Hole Spectral Function and the Relationship between Overlap Functions, Natural Orbitals and the One-Body Density Matrix in Nuclei	
The Measurements of Spin Correlation in the Reaction $dp \rightarrow pd$ (proposal)	
What Should Be Measured in Deuteron Breakup with Polarized Proton Target	
An Evidence for Collective Phenomenon in Heavy Ion Collisions at 4.2 A GeV/c	
MC Simulation of Zero Degree Calorimeter for Investigation of Pb-Pb Interaction at 160 GeV/nucleon in WA-98 Experiment	
An Algorithm for Identifying Events in the Experiment DISTO	
Determination of the Spatial Position of the Sensitive Wires in the Drift Tubes with an X-Rays Beam	

Издательский отдел ОИЯИ

ДУБНА

### Объединенный институт ядерных исследований Joint Institute for Nuclear Research

2[70]-95

# JINR RAPID COMMUNICATIONS



### ОГЛАВЛЕНИЕ CONTENTS

O развитин информационно-вычислительной инфраструктуры ОИЯИ V.V.Korenkov, V.V.Mitsyn, C.F.Ocrainets, R.H.Pose, M.Yu.Popov  JINR Informational and Computing Framework Development
A.N.Antonov, M.V.Stoitsov, M.K.Gaidarov, S.S.Dimitrova, P.E.Hodgson The Hole Spectral Function and the Relationship between Overlap Functions, Natural Orbitals and the One-Body Density Matrix in Nuclei А.Н.Антонов, М.В.Стоицов, М.К.Гайдаров, С.С.Димитрова, П.Е.Ходжсон Дырочная спектральная функция и связь между функциями перекрытия, натуральными орбиталями и одночастичной матрицей плотности ядер
I.M.Sitnik, L.S.Azhgirey, V.M.Grebenyuk, A.D.Kirillov, V.P.Ladygin, A.A.Lukhanin, N.M.Piskunov, M.P.Rekalo, V.Punjabi, C.F.Perdrisat  The Measurements of Spin Correlation in the Reaction dp → pd (proposal)  И.М.Ситник, Л.С.Ажгирей, В.М.Гребенюк, А.Д.Кириллов, В.П.Ладыгин, А.А.Луханин, Н.М.Пискунов, М.П.Рекало, В.Пунжаби, Ч.Ф.Педриза
Измерения спиновой корреляции в $dp  o pd$ реакции (проект)
A.P.Cheplakov, A.A.Kuznetsov, R.R.Mekhdiyev, M.I.Soloviev, L.M.Shcheglova, A.N.Solomin, S.Backović, D.Salihagić  An Evidence for Collective Phenomenon in Heavy Ion Collisions at 4.2 A GeV/c  А.П.Чеплаков, А.А.Кузнецов, Р.Р.Мехтиев, М.И.Соловьев, Л.М.Щеглова, А.Н.Соломин, С.Бацкович, Д.Салихагич  Наблюдение коллективных потоков  в соудареннях тяжелых нонов при 4.2 A ГэВ/с

R.Eremeev, A.Fedunov, A.Maximov, G.Shabratova,
N.Slavin, A.Vodopianov, V.Genchev
MC Simulation of Zero Degree Calorimeter for Investigation
of Pb-Pb Interaction at 160 GeV/nucleon in WA-98 Experiment
Р.Еремеев, А.Федунов, А.Максимов, Г.Шабратова,
Н.Славин, А.Водопьянов, В.Генчев
Моделирование переднего калориметра эксперимента WA-98
по исследованию взаимодействий ядер свинца со свинцом
при энергии 160 ГэВ на нуклон
M.P.Bussa, L.Fava, L.Ferrero, A.Grasso, V.V.Ivanov,
I.V.Kisel, E.V.Konotopskaya, G.B.Pontecorvo
An Algorithm for Identifying Events in the Experiment DISTO
М.П.Бусса, Л.Фава, Л.Ферреро, А.Грассо, В.В.Иванов,
И.В.Кисель, Е.В.Конотопская, Д.Б.Понтекорво
Алгоритм идентификации событий в эксперименте ДИСТО55
И.Р.Бойко, Л.С.Вертоградов, В.И.Додонов, В.В.Журавлев,
М.А.Игнатенко, З.В.Крумштейн, М.Ю.Николенко, Г.А.Шелков
Определение пространственного положения снгнальных интей
в дрейфовых трубках с помощью пучка рентгеновских квантов
I.R.Boyko, L.S. Vertogradov, V.I.Dodonov, V.V.Zhuravlev,
M.A.Ignatenko, Z.V.Krumstein, M.Yu.Nikolenko, G.A.Shelkov
Determination of the Spatial Position of the Sensitive Wires
in the Drift Tubes with an X-Rays Beam61

УДК 681.324

### О РАЗВИТИИ ИНФОРМАЦИОННО-ВЫЧИСЛИТЕЛЬНОЙ ИНФРАСТРУКТУРЫ ОИЯИ

В.В.Кореньков, В.В.Мицын, К.Ф.Окраинец, Р.Г.Позе, М.Ю.Попов

Рассмотрены основные тенденции развития систем связи, информационного и вычислительного обеспечения в ОИЯИ. Освещается текущее положение в этой области и указываются приоритетные направления развития.

Работа выполнена в Лаборатории вычислительной техники и автоматизации ОИЯИ.

### JINR Informational and Computing Framework Development

#### V.V.Korenkov et al.

Computing facilities, various information services setups, their integration with the world's sceintific community, remote resource sharing and utilization, Internet connectivity are reviewed. Current state of affairs is described and the mainstream directions for further activities are outlined.

The investigation has been performed at the Laboratory of Computing Techniques and Automation, JINR.

#### 1. Новые тенденции

В течение нескольких последних лет в прикладной информатике, особенно в той ее части, которая имеет дело с глобальными телекоммуникациями, распределенными вычислениями, моделями взаимодействия приложений, основанными на парадигме клиент — сервер, происходит замедленный, но вполне наглядный взрыв.

В особенности это становится очевидным при анализе семейства протоколов ТСР/ІР, приложений, ориентированных на это семейство, и глобальной компьютерной сети Интернет, построенной на этих протоколах. Интернет — «сеть сетей» — представляет собой прозрачное для прикладных программ объединение приблизительно 30 тыс. сетей самых различных технологий низшего уровня с числом пользователей порядка 25 млн человек. С момента своего рождения в середине 80-х годов Интернет испытывает экспоненциальный рост, удваиваясь каждый год.

Это огромное компьютерное пространство с неизбежностью превращается в средство хранения и средство доступа к практически неограниченным информационным ресурсам и, что не менее важно, в средство сотрудничества исследовательских групп

различных организаций, стран и континентов. Этому в большой степени способствует открытая архитектура сети в целом, открытые спецификации протоколов и наличие свободно-распостраняемого программного обеспечения, реализующего не только традиционный сетевой сервис (например, терминальный доступ или телеобработка), но и такие новые возможности, как аудио- и видеоконференции. По оценкам экспертов [1], около 80% ученых в развитых странах активно используют Интернет в своей деятельности.

В этом сообщении авторы хотели бы обобщить опыт, во многом носящий уникальный для России характер, построения локальной информационной структуры, включения этой структуры в глобальное инфомационное пространство и опыт использования глобальных коммуникаций для организации распределенных вычислений.

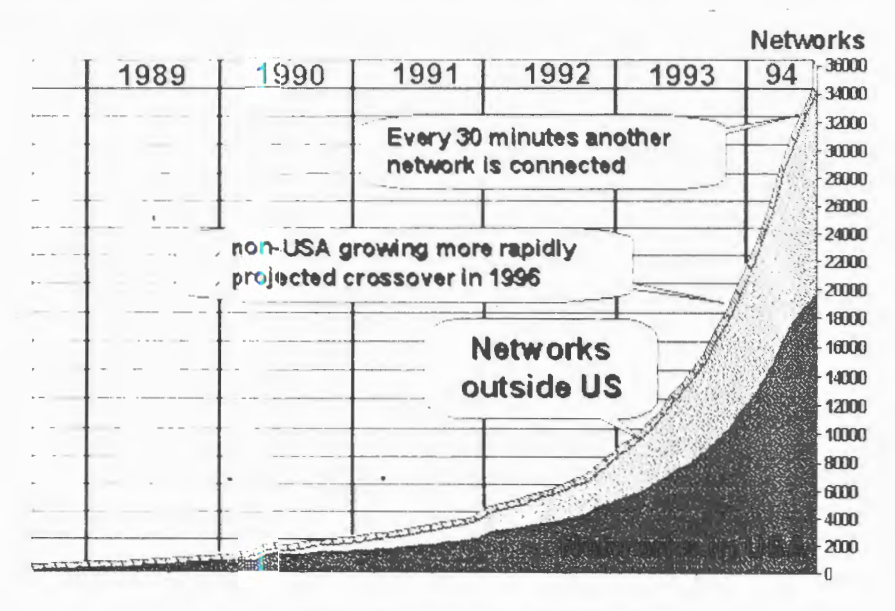


Рис.1. Рост числа сетей в Интернет

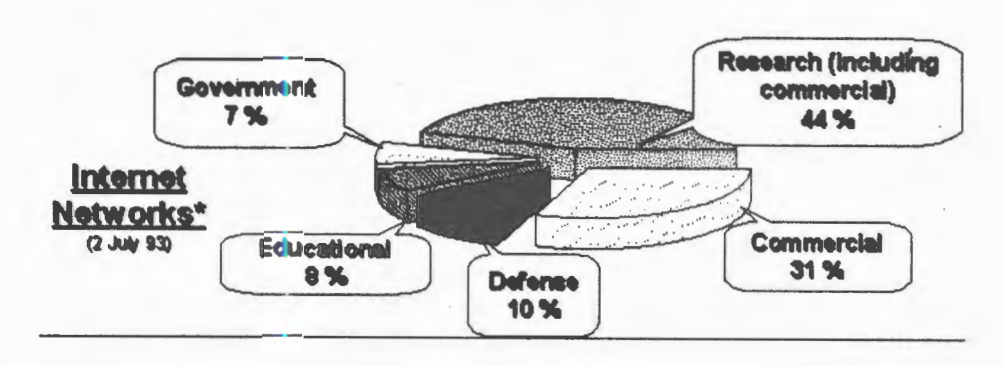


Рис.2. Структура Интернет

#### 2. Связь

Исходным и ключевым моментом для всего последующего является связь, надежная и устойчивая. В нашем случае группа сотрудников Лаборатории вычислительной техники и автоматизации, взаимодействуя с германской исследовательской сетью DFN и фирмой «Eurodata», установила в июле 1994 г. связь с Интернет, достаточную для решения широкого класса задач моделирования, обработки и графического представления информации.

Физический уровень канала Дубна — Потсдам представляет собой соединение точка — точка, использующее космическую связь и участок выделенной 4-проводной линии от места размещения спутниковой антенны в Дубне до компьютера-маршрутизатора.

На более высоком логическом уровне канал включает в себя:

- программную реализацию PPP-протокола над физическим уровнем, несущим HDLC-фреймы;
- маршрутизирующую программу GateD, реализующую протоколы IP [2], OSPF
   [3], BGP [4];
- программу NameD, обеспечивающую авторитетный (официально зарегистрированный мировыми сетевыми координационными центрами) сервис имен, адресов и сетевых услуг для зон «dubna.su» и «jinr.dubna.su», что является непременным условием работы большинства сетевых программ, например, электронной почты;
- разработанную в ОИЯИ систему контроля канала и сбора статистики, имеющую X Window System и WWW интерфейсы пользователя/оператора [8].

Таковы вкратце предпосылки, базис для дальнейшего развития.

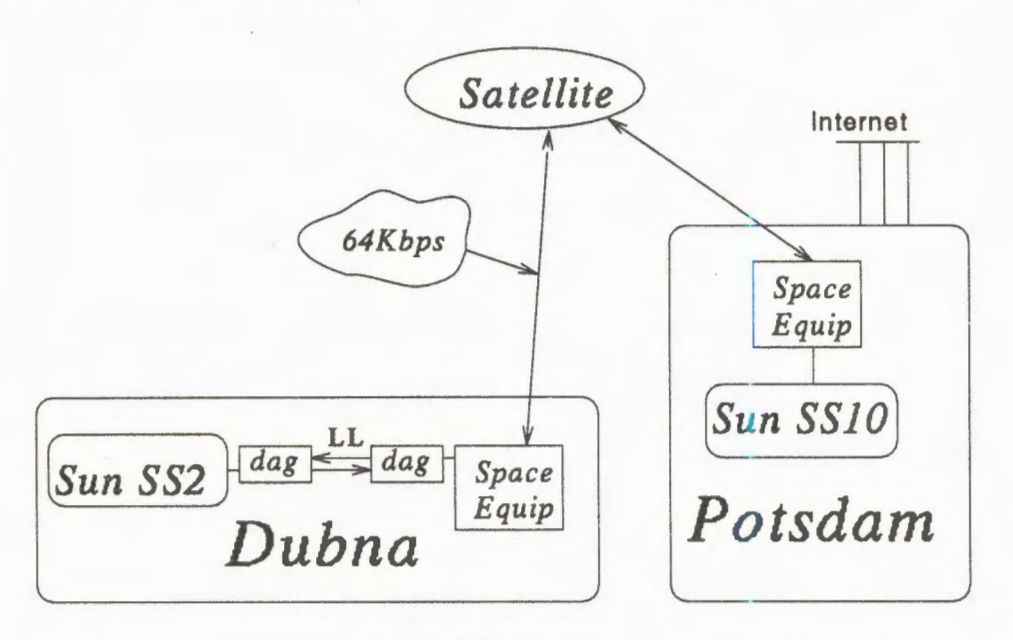


Рис.3. Схема связи

#### 3. Информационный сервис

Основой для кооперационных связей между рабочими группами исследователей, как внутри ОИЯИ, так и в рамках международных коллабораций, служит структура WWW-серверов, WWW, World Wide Web, The WEB W3, «Всемирная паутина» [5,6] — это система распределенных гипертекстовых документов, структурированных особым образом и способных включать в себя современные средства презентации объектов, такие, как графика, звук и анимация. Будучи изначально разработанным в одном из крупнейших мировых центров ядерных исследований (CERN) для нужд физиков, W3 сейчас имеет множество применений решительно во всех областях человеческой деятельности.

Первый импульс к распространению этой системы в ОИЯИ был дан в начале 1994 г. одной из первой в России инсталляций, включавшей в себя порт матообеспечения для сервера и нескольких клиентов в ConvexOS и формирование базовой гипертекстовой структуры, представляющих сведения об ОИЯИ, его лабораториях, экспериментальных установках и областях научной деятельности.

В настоящее время внутри Института насчитывается 5 серверов, предоставляющих доступ к большому количеству документов (сообщения о конференциях, статьи, документация CERN Computing & Networks Division, руководства по программным пакетам, операционным средам и т.д.) и шлюзы к различным сетевым услугам.

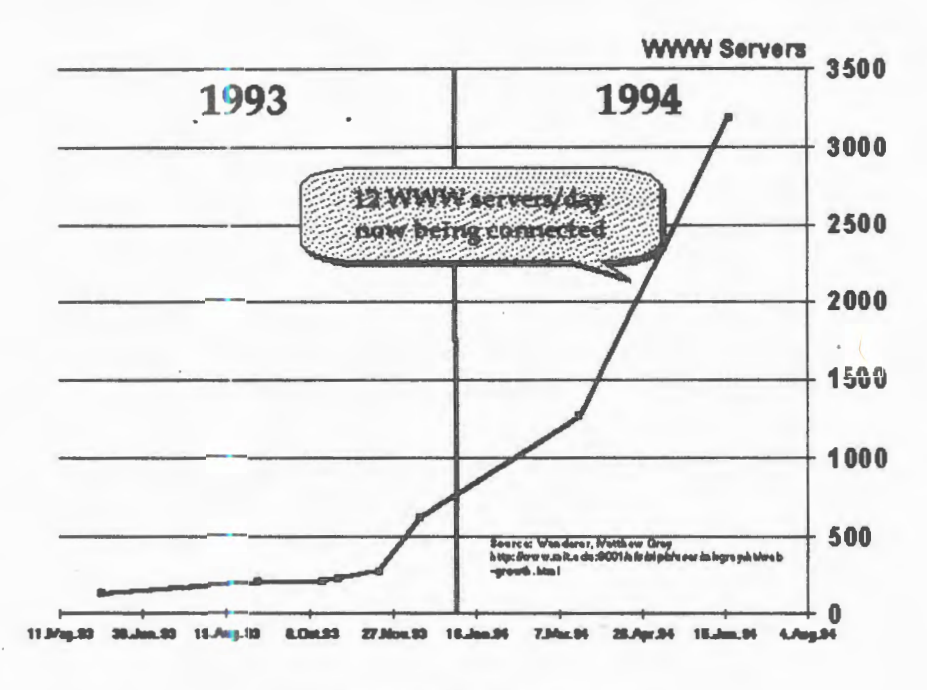


Рис.4. Рост числа WWW-серверов

Взаимодействие W3 и баз данных является актуальной областью исследований (см., напр., [9]).

По всей видимости, основным инструментом доступа пользователей исследовательских центров к информации в ближайшие несколько лет станет NCSA Mosaic — W3 — клиент для различных операционных платформ с графическим интерфейсом, прозванным «Internet killer application» за великолепные возможности и широкое распространение.

Равным образом WWW станет основным методом представления информации, начиная от конструкторской документации и заканчивая электронными публикациями.

#### 4. Распределенные вычисления

Еще один аспект доступа к глобальным ресурсам — организация удаленных и распределенных вычислений, например, разработанная в Университете штата Висконсин система Condor [7]. Как известно, во многих вычислительных центрах определенная часть ресурсов задействована не в полной мере. Проект Condor представляет собой распределенную систему автоматической (bath) обработки, в которой рабочие станции во всем мире (сейчас это 400 DEC, HP и Sparc 10) взаимодействуют, предоставляя процессорное время и иные ресурсы другим участникам во время своей недозагрузки. Естественно, администратор каждой из станций имеет полную возможность сформулировать свое собственное понимание «загруженности».

В результате, участники этой динамично развивающейся системы, не теряя ничего, приобретают возможность резко ускорить обработку своих данных, когда это становится необходимым. В настоящее время в системе Condor для физиков Института потенциально доступы следующие вычислительные платформы:

Платформа	NIKHEF	Wisconsin University
SPARC/SUNOS41	27	1
sun4m/SUNOS41	10	84
HPPAR/HPUX9		49
ALPHA/OSF1		12
MIPS/ULTRIX4.3		64
R6000/AIX32		1

Всего доступны около 250 рабочих станций.

На рис.5 представлена архитектура системы Condor, которая используется для расчетов в физике высоких энергий.

В ОИЯИ инсталлировано и используется математическое обеспечение Condor, формируется группа поддержки и развития проекта и будут предприниматься дальнейшие шаги по интеграции сетевого, информационного и вычислительного комплексов с аналогичными стуктурами исследовательских организаций во всем мире.

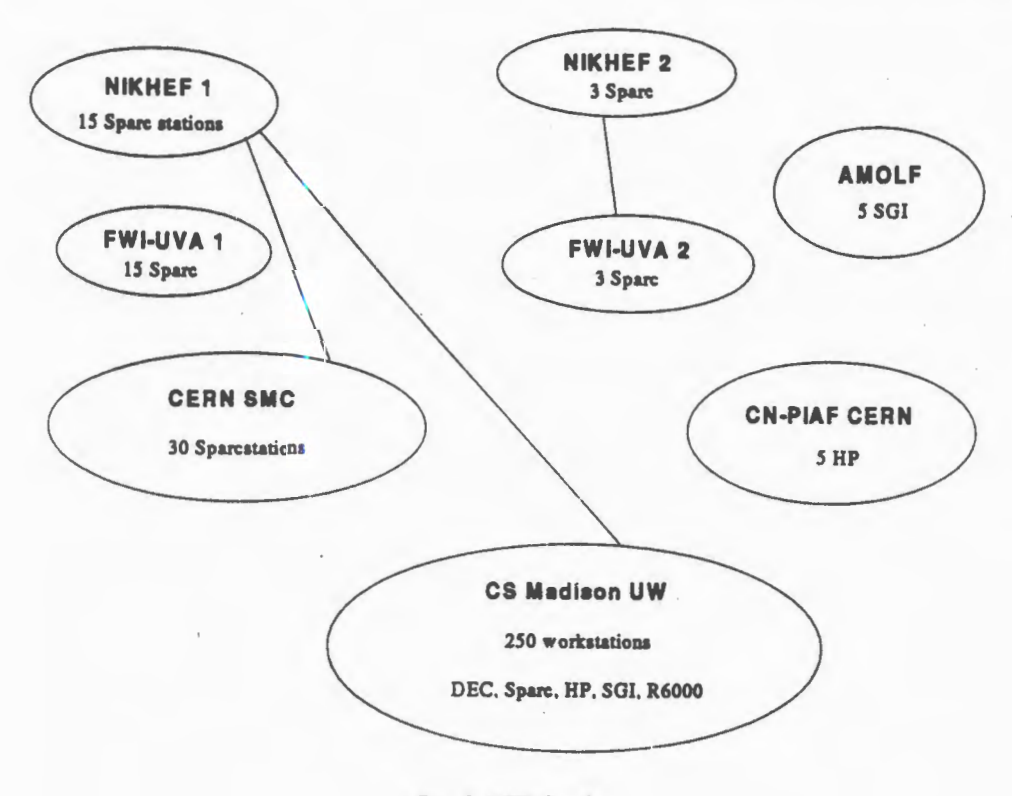


Рис.5. HEP Condor

#### Литература

- 1. Rutkowsky A. Keynote Address, Networld+Interop 94, Tokyo, June 1994.
- 2. Sympson W. The Point-to-Point Protocol (PPP), RFC1661, July 1994.
- 3. Moy J. OSPF Version 2 RFC 1583, March 1994.
- 4. Rechter Y., Di T. A Border Gateway Protocol 4, RFC 1654, July 1994.
- 5. Adie C. Network Access to Multimedia Information, RFC 1614, May 1994.
- Bernes-Lee T. Protocol for Retrieval and Manipulation of Textual and Hypermedia Information, URL=ftp://info.cern.ch/pub/www/doc/httpspec.ps, 1993.
- 7. Lizkow M., Solomon M. Supporting Checkpointing and Process Migration Outside the Unix Kernel, Usenia Winter Conference, San Francisco, 1992.

УДК 539.1.072

## THE HOLE SPECTRAL FUNCTION AND THE RELATIONSHIP BETWEEN OVERLAP FUNCTIONS, NATURAL ORBITALS AND THE ONE-BODY DENSITY MATRIX IN NUCLEI<sup>1</sup>

A.N.Antonov<sup>2</sup>, M.V.Stoitsov<sup>2</sup>, M.K.Gaidarov<sup>2</sup>, S.S.Dimitrova<sup>2</sup>, P.E.Hodgson<sup>3</sup>

A method to calculated the hole spectral function in the discrete part of the spectrum is suggested within the natural orbital representation of the one-body density matrix of A-nucleon system using its relationship with the overlap functions of the eigenstates in the (A-1)-nucleon system.

The investigation has been performed at INRNE (Bulgaria) in collaboration with Bogoliu-bov Laboratory of Theoretical Physics, JINR.

Дырочная спектральная функция и связь между функциями перекрытия, натуральными орбиталями и одночастичной матрицей плотности ядер

#### А.Н.Антонов и др.

Предложен метод для вычисления дырочной спектральной функціми для дискретной части спектра. Используется представление натуральных орбиталей одиочастичной матрицы плотности A-нуклонной системы и ее связь с функциями перекрытия для состояний (A-1)-нуклонного ядра.

Работа выполнена в ИЯИЯЭ (Болгария) в сотрудничестве с Лабораторией теоретической физики им.Н.Н.Боголюбова ОИЯИ.

#### 1. Introduction

The cross-section of direct nucleon removal processes is determined by the spectral function which contains the information on the nuclear structure and is interpreted as the probability for the removal of a nucleon with given momentum and energy from the target nucleus with A nucleons [1—16]. In particular, in the plane-wave impulse approximation the cross-section for the direct knock-out process is proportional to the diagonal element  $S(\mathbf{k}, \mathbf{k}, E) \equiv S(\mathbf{k}, E)$  of the hole spectral function (or matrix) in the momentum representation:

<sup>&</sup>lt;sup>1</sup>This work is partially supported by the Bulgarian National Science Foundation under the Contracts No.Φ-32 and Φ-406

<sup>&</sup>lt;sup>2</sup>Institute of Nuclear Research and Nuclear Energy, Bulgarian Academy of Sciences, Sofia 1784, Bulgaria <sup>3</sup>Nuclear Physics Laboratory, Department of Physics, University of Oxford, Oxford OX1-3RH, U.K.

$$S(\mathbf{k}, \mathbf{k}'; E) = \langle \Psi_0 | a^+(\mathbf{k}') \delta(E + \hat{H} - E_A^0) a(\mathbf{k}) | \Psi_0 \rangle, \tag{1}$$

where  $|\Psi_0\rangle$  is the ground state wave function of the target nucleus with A nucleons,  $a^+(\mathbf{k}')$  and  $a(\mathbf{k})$  are creation and annihilation operators for a nucleon with momentum  $\mathbf{k}'$  and  $\mathbf{k}$ , respectively,  $\hat{H}$  is the Hamiltonian of the system with (A-1)-nucleons and  $E_A^{\ 0}$  is the ground state energy of the target nucleus. If the latter has a total spin and parity  $J^{\pi}=0^+$ , then introducing a complete set of eigenstates of  $\hat{H}$  for the system of (A-1)-nucleons  $|\Psi_f\rangle$  (where the state  $|\Psi_f\rangle$  is characterized by the energy  $E_f$  with both discrete and continuous values and by other discrete and continuous quantum numbers) the hole spectral function can be written in the form:

$$S\left(\mathbf{k},\,\mathbf{k}',\,E\right) = \left\langle\;\Psi_{0}\;|a^{\dagger}(\mathbf{k}')|\Psi_{f}\;\right\rangle\left\langle\Psi_{f}\;|a(\mathbf{k})|\Psi_{0}\;\right\rangle\;\delta\;(E+E_{f}-E_{A}^{\;0}), \tag{2}$$

$$\equiv \Phi_f^*(\mathbf{k}') \Phi_f(\mathbf{k}) \delta(E + E_f - E_A^0), \tag{3}$$

where

$$\Phi_{f}(\mathbf{k}) \equiv \langle \Psi_{f} | a(\mathbf{k}) | \Psi_{0} \rangle \tag{4}$$

is the overlap function in the momentum representation [17-19].

The methods used to calculated the spectral function are reviewed, e.g., in [7,14,16]. The use of the independent-particle shell model (when the overlap function (4) is equal to the single-particle wave function of the occupied state) cannot explain the fragmentation or spreading of the hole strength. This is because, due to the residual interaction, the hole state in the target nucleus is not an eigenstate of the (A-1)-nucleon system and its strength is distributed over several states of the final system. The structure of the spectral function has been studied in the framework of the Green function method [1,20]. The detailed analyses have been carried out by expanding the mass operator into a perturbation series [1,3,4, 20,21]. Calculations using continuum shell model with residual interactions were given in [5,22]. The nucleon-nucleon correlation effects on the spectral functions were studied with the Green function method in [23—27,13]. It was shown that the overlap functions can be determined by a Schrödinger type equation in the discrete [8,12] and continuous [12] spectrum of the Hamiltonian for the (A - 1)-body residual nucleus. The deep-hole nuclear levels and their large widths established from (e, e', p) and (p, 2p) reactions have been considered within the many-body field theory without any model approaches in [26]. The Hartree-Fock method using Skyrme forces has been applied to calculate the proton hole-spectral function in [28].

In this work we use the natural orbital representation of the one-body density matrix (OBDM) in A-nucleon system [29]. In this representation the OBDM is diagonalized by the so-called natural orbitals (NO) which form a complete orthonormal set of functions. An expansion of the overlap functions (4) in the basis of the natural orbitals is used. We suggest a method to calculate the hole spectral functions using essentially the NO and overlap functions and their relationship with the OBDM. The following two reasons can justify the use of the method:

1) Recently the diagonalization of the realistic one-body density matrix of the correlated nuclear ground state obtained by various correlation methods [16], such as the

Jastrow method [30—32], as well as the generator coordinate method [16,33,34] and the coherent density fluctuation model [16,34,35] gave reliable information on the natural orbitals and occupation numbers in nuclei. These quantities correspond to the realistic behaviour of nuclear characteristics which are sensitive to the short-range nucleon-nucleon correlations, such as the nucleon and cluster momentum distributions, the mean kinetic and removal energies, radii and others. The natural orbitals in nuclei, as well as those in other fermion systems, such as  ${}^{3}$ He liquid drops [36], are strongly localized and quite different from the overlap functions and from the mean-field type orbitals [30,34,36,37]. Thus, it is of importance to apply the natural orbitals corresponding to realistic OBDM obtained in correlation theoretical methods to calculate the hole spectral function  $S(\mathbf{k}, \mathbf{k}', E)$ .

2) The basic quantity which is necessary to calculate the spectral function (3) is the overlap function (4). We show in this paper that the hole spectral function in the discrete part of the spectrum can be calculated by using the general relationship [37] which connects the asymptotic behaviour of the one-body density matrix with the overlap functions of the (A-1)-particle system eigenstates. This relationship is of general importance because it enables one to obtain quantities connected with the bound eigenstates of the (A-1)-particle system (such as overlap functions, spectroscopic factors and separation energies) by means of the exact OBDM (or by a realistic one obtained in a given correlation method) of the ground state of the A-particle system. In this way, the hole spectral function in the discrete part of the spectrum can be, in principle, calculated on the basis of the OBDM of the A-particle system.

In Section 2 we introduce the necessary quantities which are used in the theoretical method to calculate the hole spectral function. The method is given in Section 3.

### 2. The Hole Spectral Function and the Natural Orbital Representation in Nuclei

The one-body density matrix (OBDM) of the ground state  $|\Psi_0\rangle$  of the A-nucleon system has the form

$$\rho\left(x,x'\right) = \left\langle \left.\Psi_{0}\right| a^{+}(x) \; a(x') | \; \Psi_{0} \; \right\rangle, \tag{5}$$

where  $x = \{rot\}$  labels spatial, spin and isospin coordinates and  $a^{+}(x)$ , a(x') are the creation and annihilation operators.

The natural orbitals (NO)  $\varphi_a(x)$  are defined [29] as the complete orthonormal set of single-particle wave functions which diagonalize the OBDM:

$$\rho (x, x') = \sum_{a} N_a \phi_a^*(x) \phi_a(x').$$
 (6)

The eigenvalues  $N_a$  ( $0 \le N_a \le 1$ ,  $\sum_a N_a = A$ ) are the natural occupation numbers. We note that the sum (6) is over the discrete states determined by the finite-range NO  $\varphi_a(\mathbf{k})$ .

The OBDM (5) can be presented also in the form:

$$\rho(x, x') = \sum_{f} \Phi_f^*(x) \Phi_f(x'), \qquad (7)$$

where  $\Phi_f(x) = \langle \Psi_f | a(x) | \Psi_f \rangle$  is the overlap function in the coordinate representation.

The overlap functions can be expanded in the basis of the natural orbitals (e.g., in momentum space):

$$\Phi_{f}(\mathbf{k}) = \sum_{a} \langle \varphi_{a} | \Phi_{f} \rangle \varphi_{a}(\mathbf{k}). \tag{8}$$

The hole spectral function is then given by the expression:

$$S(\mathbf{k}, \mathbf{k}', E) = \sum_{a,b} \varphi_a^*(\mathbf{k}') \varphi_b(\mathbf{k}) \sum_f \langle \Phi_f | \varphi_a \rangle \langle \varphi_b | \Phi_f \rangle \delta(E + E_f - E_A^0) \equiv$$

$$\equiv \sum_{a,b} \varphi_a^*(\mathbf{k}') \varphi_b(\mathbf{k}) S_{ab}(E), \tag{9}$$

where

$$S_{ab}(e) \equiv \sum_{ab} \langle \Phi_f | \Phi_a \rangle \langle \Phi_b | \Phi_f \rangle \delta (E + E_f - E_A^0). \tag{10}$$

The quantity (for which different notations exist, e.g., [14,15]):

$$\theta_{af} \equiv S_{af}^{1/2} \equiv \langle \phi_a | \Phi_f \rangle \tag{11}$$

from (8) and (9) is the amplitude for the contribution of the orbital a to the overlap function for the eigenstate  $|\Psi_f\rangle$ . We mention that the quantity (11) determines both the spectroscopic factor of the state  $|\Psi_f\rangle$  [19]

$$S_f^{A-1} \doteq \langle \Phi_f | \Phi_f \rangle = \sum_a |\theta_{af}|^2 = \sum_a S_{af} = \sum_a |\langle \varphi_a | \Phi_f \rangle|^2$$
 (12)

and the occupation probability of the orbital a:

$$\delta_a' := \iint_a |\theta_{af}|^2 = \iint_a S_{af} = \iint_a |\langle \varphi_a | \Phi_f \rangle|^2.$$
 (13)

In general, for a given orbital a, only a limited subset of states f of the residual nucleus contribute to the sums (10) and (13).

The function  $S_{ab}(E)$  (given by Eq.(10) and often called also «spectral function») can be rewritten [5] introducing the different states  $|\Psi_f\rangle$  of the residual nucleus: i) the bound states  $|\Psi_{E_{\nu},\alpha}\rangle$  with energy  $E_{\nu}$  and degeneracy quantum number  $\alpha$ , and ii) the continuum states  $|\Psi_{E_{\mu},\alpha}\rangle$  with energy  $E_{f}$  and the channel index c which specifies the channel where there is an incoming wave (all other channels contain only outgoing waves), as well as all degeneracies like spin projections, etc. Then Eq.(10) becomes:

$$S_{ab}(E) = \sum_{v, \alpha} \langle \Phi_{v\alpha} | \Phi_{a} \rangle \langle \Phi_{b} | \Phi_{v\alpha} \rangle \delta (E + E_{v} - E_{A}^{0}) +$$

$$+\sum_{c} \langle \Phi_{E_{f}^{-}E_{A}^{0}-E_{c}}| \varphi_{a} \rangle \langle \varphi_{b}| \Phi_{E_{f}^{-}E_{A}^{0}-E_{c}} \rangle \theta (E_{A}^{0}-E_{A-1}^{thr}-E) \equiv$$

$$\equiv S_{ab}^{d,s}(E) + S_{ab}^{c.s.}(E), \tag{14}$$

where  $\Phi_{v\alpha}$  and  $\Phi_{E_f}$ , c are the overlap functions associated with the bound and continuum eigenstates of the residual nucleus and  $E_{A-1}^{thr}$  is the threshold for particle decay of this nucleus. If the latter is a nucleon threshold, then  $E_{A-1}^{thr} = E_{A-2}^{0}$ , where  $E_{A-2}^{0}$  is the ground-state energy of the nucleus with A-2 nucleons [5]. The hole-spectral function (14) contains two parts: i) the spectral function in the discrete part of the spectrum  $S_{ab}^{d.s.}$  (E), and ii) the spectral function in the continuum of the hole spectrum  $S_{ab}^{c.s.}$  (E) with  $E \leq E_A^{0} - E_{A-2}^{0}$ .

#### 3. The Theoretical Method

The hole spectral function (Eqs. (9) and (14)) is essentially connected with the natural orbitals  $\{\varphi_a\}$  and the overlap functions  $\Phi_f$  and their relationship with the OBDM. Firstly, we shall outline briefly this relationship.

In the case of spherical symmetry the overlap functions have the form:

$$\Phi_f^{(q)}(x) = \Phi_f^{(qlj)}(r) Y_{ljm}(\Omega, \sigma), \tag{15}$$

where  $\Phi_f^{(qlj)}(r)$  is the radial part,  $Y_{ljm}(\Omega, \sigma)$  is the spin-angular function, q denotes the nature (proton and neutron) of the overlap function and l, j are angular and total momentum quantum numbers. Substituting Eq. (15) in Eq. (7), the OBDM can be written as:

$$\rho(x, x') = \sum_{qlj} \rho^{(qlj)}(r, r') \sum_{m} Y_{ljm}^{*}(\Omega, \sigma) Y_{ljm}(\Omega', \sigma'),$$
(16)

where the radial part of the OBDM is:

$$\rho^{(qlj)}(r, r') = \sum_{f} \Phi_f^{(qlj)}(r) \Phi_f^{(qlj)}(r'). \tag{17}$$

It is known [19] that the overlap functions associated with the bound states of the (A-1)- and (A+1)-nucleon systems are eigenstates of a single-particle Schrödinger equation in which the mass operator plays the role of a potential. Due to the finite range of the mass operator, the asymptotic behaviour of the radial part of the neutron overlap functions for bound states  $\nu$  (labeled by  $\nu = 0, 1, \ldots$  with increasing energy) of the (A-1)-nucleon system is given by [17,18,37]:

$$\Phi_{v}^{(qlj)}(r) \to C_{v}^{(qlj)} \exp\left(-k_{v}^{(qlj)}r\right)/r, \tag{18}$$

where

$$k_{V}^{(qlj)} = \frac{1}{\pi} \left[ 2m_{q} \left( E_{V}^{(qlj)} - E_{A}^{0} \right) \right]^{1/2}. \tag{19}$$

For protons some mathematical complications arise due to an additional long-range part originating from the Coulomb interaction [18], though everything from the neutron case remains valid. It is assumed in [37] that Eq. (18) is also valid for the overlap functions corresponding to the (A-1) continuum.

The asymptotic form of the overlap functions (Eqs. (18) and (19)) determines the asymptotic behaviour of the radial part of the OBDM [37]. Since higher excited states have faster decay, at large values of  $r' \equiv a \rightarrow \infty$  one gets:

$$\rho^{(qlj)}(r, a) \to \Phi_0^{(qlj)}(r) C_0^{(qlj)} \exp(-k_0^{(qlj)}a)/a.$$
 (20)

The normalization coefficient  $C_0^{(qlj)}$  can be obtained from the asymptotic form of the diagonal part of the radial OBDM:

$$\rho^{(qlj)}(a, a) \to |C_0^{(qlj)}|^2 \exp(-2k_0^{(qlj)}a)/a^2.$$
 (21)

By means of Eqs. (20) and (21) one can derive the lowest bound state overlap function

$$\Phi_0^{(qlj)}(r) = \frac{\rho^{(qlj)}(r, a)}{C_0^{(qlj)}\exp(-k_0^{(qlj)}a)/a},$$
(22)

as well as the separation energy

$$\varepsilon_0^{(qlj)} = \hbar^2 k_0^{(qlj)^2} / 2m_q \tag{23}$$

and the spectroscopic factor

$$S_0^{(qlj)} = \langle \Phi_0^{(qlj)} | \Phi_0^{(qlj)} \rangle. \tag{24}$$

As shown in [37], the overlap functions for all bound states of the (A-1)-nucleon system can be constructed from the OBDM repeating the above procedure. For instance, the overlap function for the next bound state is:

 $\Phi_{1}^{(qlj)}(r) = \frac{\rho^{(qlj)}(r, a) - \Phi_{0}^{(qlj)}(r) \Phi_{0}^{(qlj)}(a)}{C_{1}^{(qlj)} \exp(-k_{1}^{(qlj)}a)/a}.$  (25)

In the case of the continuum contributions to the OBDM one can calculate the particular sum over the scattering channels  $c: \sum_{c} [\Phi_{c}^{(qlj)}(r, E) C_{c}(E)]$ , but not the overlap function

tion for each channel [37].

The method for calculating of the hole spectral function in the discrete part of the spectrum (for non-degenerate states v):

$$S^{d.s.}(\mathbf{k}, \mathbf{k}', E) = \sum_{a,b} \varphi_a^*(\mathbf{k}') \varphi_b(\mathbf{k}) \sum_{v} \langle \Phi_v | \varphi_a \rangle \langle \varphi_b | \Phi_v \rangle \delta (E + E_v - E_A^0)$$
 (26)

from a given theoretical correlation method, consists in the following procedure:

1) By diagonalizing the one-body density matrix of the A-particle system ground state one obtains the natural orbitals  $\{\phi_a(\mathbf{k})\}$  (e.g., as in [30—35,16]);

- 2) The bound-state overlap functions  $\Phi_{v}$  and separation energies  $\epsilon_{v}$  are calculated on the basis of the one-body density matrix following the approximate method described above (Eqs.(20)—(25)).
- 3) The amplitudes of the contribution of the natural orbital a to the overlap function  $\langle \varphi_a | \Phi_v \rangle$  are calculated and the results substituted in Eq.(26).

It can be seen from Eqs.(1) and (5) that the energy integral of the hole spectral function (1) defines the one-body density matrix in the momentum representation

$$\int_{-\infty}^{E_F} dES(\mathbf{k}, \mathbf{k}', E) = \rho(\mathbf{k}, \mathbf{k}'),$$
(27)

where  $E_F^-$  is a negative quantity whose absolute value is equal to the separation energy of the A-nucleon system [19].

We emphasize that the method described above enables one to obtain the hole spectral function in the discrete part of the spectrum (i.e., the integrand of the left-hand side of Eq.(27) in the energy interval between  $E_A^0 - E_{A-2}^0$  and  $E_F^-$ ) on the basis of the one-body density matrix calculated in a given correlation method. The knowledge of  $\rho$  (k, k') can give some information on the remaining part of the integrand in the left-hand side of Eq.(27), namely the hole spectral function in the continuum part of the spectrum in the energy interval between  $-\infty$  and  $E_A^0 - E_{A-2}^0$ .

In this paper we suggest a new theoretical method to obtain the hole spectral function in the discrete part of the spectrum. The method is based on the natural orbital representation in nuclear theory and uses essentially both the natural orbitals and overlap functions as well as their relationship with the OBDM. Thus the theoretical point of the method consists in the possibility of using the OBDM which is related to the properties of the A-nucleon system to calculate the hole spectral function which determines the cross-section of the nucleon removal processes and gives information on the structure of the (A-1)-nucleon system. The applications of the method can serve also as a test of the predictions of the correlated methods concerning the OBDM of the correlated ground state of the A-nucleon system.

Our program to apply the suggested method includes two stages: i) calculations of overlap functions on the basis of realistic OBDM from a given correlation method and studies of their properties, and ii) calculations of hole spectral functions in the discrete part of the spectrum and comparison with available experimental data. The results from the fulfilment of this program will be given elsewhere.

#### References

- 1. Gross D.H.E., Lipperheide R. Nucl. Phys., 1970, A150, p.449.
- 2. Jacob G., Maris Th.A.J. Rev. Mod. Phys., 1973, 45, p.6.
- 3. Wille U., Gross D.H.E., Lipperheide R. Phys. Rev., 1971, C4, p.1070.
- 4. Wille U., Lipperheide R. Nucl. Phys., 1972, A189, p.113.

- 5. Fritsch W., Lipperheide R., Wille U. Nucl. Phys., 1972, A198, p.515.
- 6. Hodgson P.E. Rep. on Progr. in Physics, 1975, 38, p.847.
- 7. Dieperink A.E.L., T. de Forest Jr. Ann. Rev. Nucl. Sci., 1975, 25, p.1.
- 8. Boffi S., Capuzzi F. Lett. Nuovo Cim., 1979, 25, p.209.
- 9. Boffi S., Giusti C., Pacati F.D., Frullani S. Nucl. Phys., 1979, A319, p.461.
- 10. Ciofi degli Atti C. Progr. in Part. and Nucl. Phys., 1980, 3, p.163.
- Boffi S., Molinari A. In: Proceedings of the International School of Physics «Enrico Fermi», Course LXXIX., Varenna 1980, North-Holland Publ. Company, Amsterdan — New York — Oxford, 1981, p.373.
- 12. Boffi S., Capuzzi F. Nucl. Phys., 1981, A351, p.219.
- 13. Antonov A.N., Nikolaev V.A., Petkov I.Zh. Z. Phys., 1982, A304, p.239.
- 14. Frullani S., Mougey J. Adv. Nucl. Phys., 14, Plenum Press, New York, 1984, p.1.
- 15. Dean G.W.R., Brussaard P.J. Z. Phys., 1986, A323, p.351.
- Antonov A.N., Hodgson P.E., Petkov I.Zh. Nucleon Correlations in Nuclei, Springer-Verlag, Berlin Heidelberg New York, 1993, p.1.
- 17. Berggren T. Nucl. Phys., 1965, 72, p.337.
- 18. Bang J.M., Gareev F.A., Pinkston W.T., Vaagen J.S. Phys. Rep., 1985, 125, p.253.
- 19. Mahaux C., Sartor R. Adv. Nucl. Phys., 20, Plenum Press, New York, 1991, p.1.
- 20. Engelbrecht C.A., Weidenmuller H.A. Nucl. Phys., 1972, A184, p.385.
- 21. Faessler A., Kusuno S., Strobel G.L. Nucl. Phys., 1973, A203, p.513.
- 22. Fritsch W., Lipperheide R., Wille U. Phys. Lett., 1973, 45B, p.103.
- 23. Orland H., Schaeffer R. Nucl. Phys., 1978, A299, p.442.
- 24. Ramos A., Polls A., Dickhoff W.H. In: The Nuclear Equation of State, Part A, ed. by W.Greiner and H.Stocker, Plenum Press, New York, 1989.
- 25. Sartor R. Nucl. Phys., 1976, A267, p.29; 1977, A289, p.329.
- Vagradov G.M., Gorchakov V.V. Particles and Nuclei, 1974, 5, p.308;
   Vagradov G.M., Gareev F.A., Bang J. Nucl. Phys., 1977, A278, p.319.
- 27. Sartor R., Mahaux C. Phys. Rev., 1980, C21, p.2613.
- 28. Van Neck D., Warcquier M., Ryckebusch J. Phys. Lett., 1990, 249B, p.157.
- 29. Lowdin P.-O. Phys. Rev., 1955, 97, p.1474.
- Stoitsov M.V., Anionov A.N., Dimitrova S.S. Phys. Rev., 1993, C47, p.R455;
   Phys. Rev. 1993, C48, p.74.
- 31. Stoitsov M.V., Antonov A.N. Z. Phys., 1993, A345, p.259.
- 32. Stoitsov M.V., Antonov A.N., Dimitrova S.S. Z. Phys., 1993, A345, p.359.
- 33. Antonov A.N., Bonev I.S., Christov C.V., Nikolov E.N., Petkov I.Zh. Nuovo Cim., 1990, A103, p.1287.
- 34. Antonov A.N., Kadiev D.N., Hodgson P.E. Phys. Rev., 1994, C50, p.164.
- 35. Antonov A.N., Christov C.V., Nikolov E.N., Petkov I.Zh., Hodgson P.E. Nuovo Cim., 1989, A102, p.17'01.
- 36. Lewart D.S., Pandharip and V.R., Pieper S.C. Phys. Rev., 1988, B37, p.4950.
- 37. Van Neck D., Waroquier M., Heyde K. Phys. Lett., 1993, B314, p.255.

УДК 539.128.417

### THE MEASUREMENTS OF SPIN CORRELATION IN THE REACTION dp $\rightarrow pd$ (PROPOSAL)

I.M.Sitnik, L.S.Azhgirey, V.M.Grebenyuk, A.D.Kirillov, V.P.Ladygin, A.A.Lukhanin, N.M.Piskunov, M.P.Rekalo<sup>1</sup>, V.Punjabi<sup>2</sup>, C.F.Perdrisat<sup>3</sup>

Recent measurements of the polarization observables in the reaction  $dp \rightarrow pd$  at Dubna and Saclay are reviewed. It is shown that new polarization observables need to be measured. Effects due to the polarization of the interacting particles are considered. It is shown that a previously unobserved polarization characteristic, namely the spin correlation due to the transverse polarization of beam and target particles is sensitive to possible P-wave components in the deuteron. We propose to carry out the measurements of this spin-correlation observable in Dubna. It will be an important step in the completion of a program to obtain all independent polarization observables in backward elastic scattering.

The investigation has been performed at the Laboratory of High Energies, JINR.

#### Измерения спиновой корреляции в dp → pd реакции (проект)

#### И.М.Ситник и др.

Дан обзор недавних измерений поляризационных характеристик реакции  $dp \to pd$  в Дубне и Сакле. Показана необходимость измерения новых поляризационных характеристик этой реакции. В этой связи рассмотрены эффекты, связанные с поляризацией обеих начальных частиц. Показано, что не измерявшаяся ранее поляризационная характеристика, а именно спиновая корреляция при поперечной векторной поляризации обеих начальных частиц, чувствительна к возможному существованию P-волновых компонент в дейтроне. Рассмотрена возможность проведения таких измерений в Дубне. Это будет важный шаг в выполнении программы полного эксперимента для реакции упругого dp-рассеяния назад.

Работа выполнена в Лаборатории высоких энергий ОИЯИ.

#### 1. Introduction

The dp backward elastic scattering (BES) is one of the classic reactions to obtain infromation about the deuteron structure. The matter is in the framework of the Impulse Approximation (IA), there is one-to-one connection between the only kinematical parameter of this reaction, s, and the argument of the deuteron wave function (DWF) in the momen-

<sup>&</sup>lt;sup>1</sup>National Science Center — Kharkov Institute of Physics and Technology, 310108 Kharkov, Ukraine

<sup>&</sup>lt;sup>2</sup>Norfolk State University, Norfolk, USA

<sup>&</sup>lt;sup>3</sup>College William & Mary, Williamsburg, USA

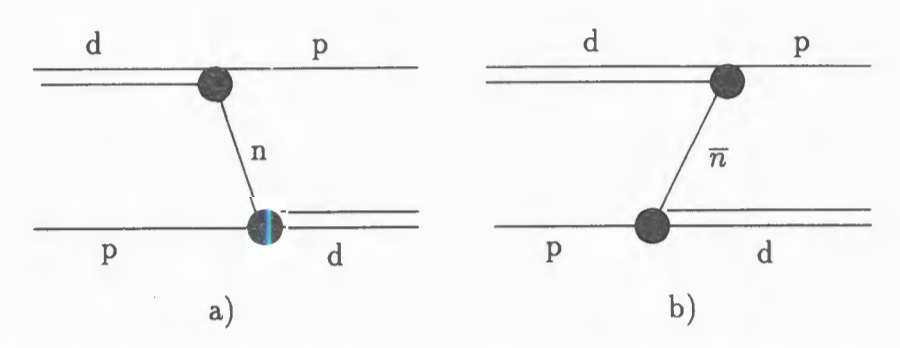


Fig.1. The IA diagrams for the p(d, p) d reaction: a) exchange by the neutron; b) exchange by the antineutron

tum space, when the deuteron is implied as two-nucleon system. That is a serious advantage of this reaction (and of the deuteron electrodisintegration also) in comparison with ed elastic scattering, where observables are connected with argument of the DWF through integral.

The differential cross section and the tensor analysing power  $T_{20}$  were measured in the GeV range at SATURNE I a long time ago (see Ref.[1] and Refs. therein, and [2], respectively).

Usually this reaction is considered as the one-neutron-exchange (ONE) process (Fig.1a), which is a particular case of the IA.

Of course, one does not expect that such a simple approach is valid at large internal momenta, when the 6-q rather than the two-nucleon picture of the deuteron structure is relevant. Therefore investigation of this reaction up to the maximal energy available is of central importance to the sudy of the deuteron structure at small distances.

#### 2. Status of Investigations of BES

The momentum densities extracted from electro-disintegration data [3] and from the dp backward scattering [1] usng an approach [4] (Fig.2) demonstrate a good agreement with one another, in spite of a substantial discrepancy with the IA predictions using standard DWF. This agreement between electron and proton data constitutes a solid foundation, indicating that BES pd is a reliable source of information about the deuteron structure. Therefore the study of polarization observables of this reaction seems to be very attractive because of much more counting rate in comparison with the investigation of the same problem using electron probe.

The polarization observables of BES  $T_{20}$  and the deuteron to proton polarization transfer coefficient  $\kappa_0$  have simple expressions in the IA approach when written in terms of the DWF components u(k) (S-vave) and w(k) (D-wave) [5,6,8]; for  $T_{20}$  the relation is:

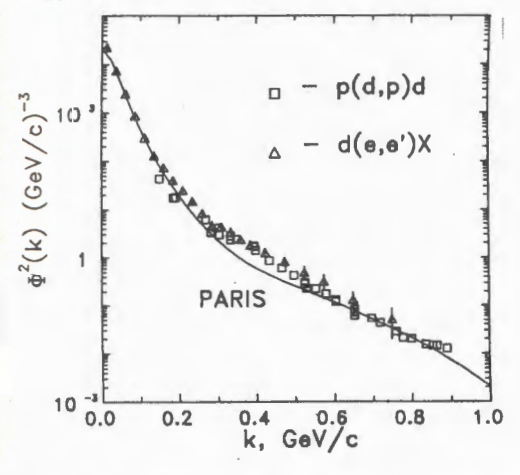
$$T_{20} = \frac{1}{\sqrt{2}} \frac{\sqrt{8}uw - w^2}{u^2 + w^2} = -\sqrt{2} \frac{x^2 - 1}{x^2 + 2},$$
 (1)

where x = 1 + b(k)/a(k),  $a(k) = u(k) + w(k)/\sqrt{2}$  and  $b(k) = -3w(k)/\sqrt{2}$ , k is internal momentum of nucleons in the deuteron.

For the polarization transfer coefficient it is:

$$\kappa_0 = \frac{u^2 - w^2 - uw/\sqrt{2}}{u^2 + w^2} = \frac{3x}{x^2 + 2} \ . \tag{2}$$

It was shown in [7] that one can eliminate u and w and obtain a connection between  $\kappa_0$  and  $T_{20}$  which does not depend upon the particular DWF:



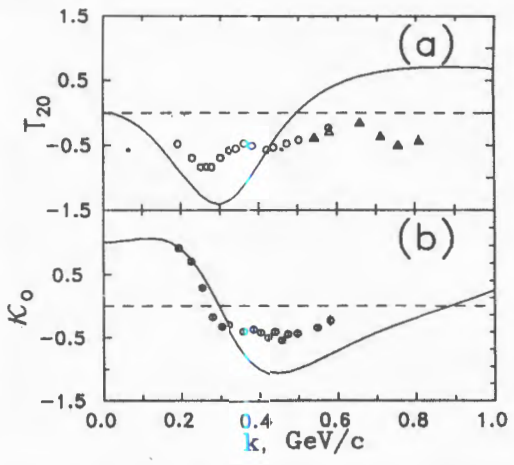


Fig.2. The momentum distributions of nucleons extracted from the *dp* backward scattering [1] and electrodisintegration data [3]

Fig.3. a)  $T_{20}$  data [9,10] versus Infinite Momentum Frame variable k; b)  $\kappa_0$  data [10] versus k

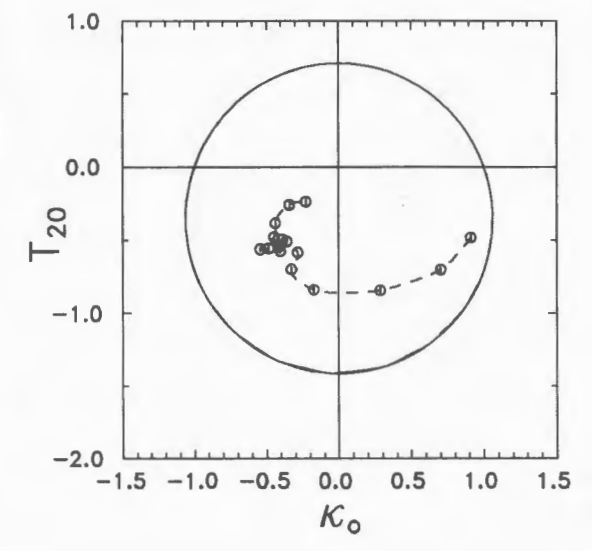


Fig.4. Correlation between  $T_{20}$  and  $\kappa_0$  in backward elastic scattering

$$\kappa_0^2 + \left(T_{20} + \frac{1}{2\sqrt{2}}\right)^2 = \frac{9}{8}$$
 (3)

The Virginia-Dubna-Saclay collaboration was conceived in 1991 to measure the polarization observables  $T_{20}$  and  $\kappa_0$  in the  $dp \to pd$  reaction and the data were obtained in Saclay in 1992—93 [10]. The measurement of the tensor analysing power  $T_{20}$  was continued to larger energies in Dubna [9]. The combined  $T_{20}$  data are shown in Fig.3a, and the Saclay data for  $\kappa_0$  are presented in Fig.3b.

The principal contradiction of the data [10] with the circle (3) in a  $(T_{20} - \kappa_0)$  correlation plot (Fig.4) demonstrates that at least one of two main assumptions (namely that the ONE diagram dominates, and the DWF contains S- and D-wave only) is not correct [10]. In Ref. [7] it is shown that similar correlation and deviation from the IA circle (3) takes place for the p(d, p) X reaction. To say more let us try to consider the dp backward elastic scattering in a model independent approach.

#### 3. General Analysis of BES

In general, dp elastic scattering can be described by 12 complex amplitudes. That means one needs to measure at least 23 polarization observables [12] to reconstruct all amplitudes. Due to P-invariance of strong interaction and total helicity conservation BES (as well as  $0^{\circ}$  scattering) can be described by only four independent complex amplitudes for the following transition  $\lambda_d$ ,  $\lambda_p \to \lambda_d'$ ,  $\lambda_p'$ ,

$$\begin{split} F_{0+ \to 0+} &= g_2(s), \\ F_{++ \to ++} &= g_1(s) + g_4(s), \\ F_{-+ \to -+} &= g_1(s) - g_4(s), \\ F_{0+ \to +-} &= -\sqrt{2}g_3(s), \end{split}$$

where  $F_{\lambda_d,\lambda_p\to\lambda_d',\lambda_p'}$  are helicity and  $g_1-g_4$  are the so-called scalar amplitudes, which are complex in the general case. Therefore only 7 polarization observables must be measured to reconstruct all of them.

The general spin structure of this reaction can be written in the following form [5]

$$\mathcal{M} = \chi_{2}^{\dagger} F \chi_{1}, \qquad F = A + i \sigma \cdot \mathbf{B},$$

$$A = g_{1}(s) \left[ \mathbf{U}_{1} \mathbf{U}_{2}^{*} - (\mathbf{n} \mathbf{U}_{1}) (\mathbf{n} \mathbf{U}_{2}^{*}) \right] + g_{2}(s) (\mathbf{n} \mathbf{U}_{1}) (\mathbf{n} \mathbf{U}_{2}^{*}),$$

$$\mathbf{B} = g_{3}(s) \left[ \mathbf{U}_{1} \times \mathbf{U}_{2}^{*} - \mathbf{n} (\mathbf{n} \mathbf{U}_{1} \times \mathbf{U}_{2}^{*}) \right] + g_{4}(s) \mathbf{n} (\mathbf{n} \mathbf{U}_{1} \times \mathbf{U}_{2}^{*}), \tag{4}$$

where  $\mathbf{U}_1$  ( $\mathbf{U}_2$ ) is the initial (final) deuteron spin vector,  $\mathbf{\chi}_1$  ( $\mathbf{\chi}_2$ ) is the two-component spinor of the initial (final) proton,  $\mathbf{\sigma}$  are the Pauli matrices, s is the Mandelstam's variable (squared total energy). The parametrization (4) is valid for any mechanism of the discussed reaction.

For any form of the Impulse Approximation (ONE + exchange of any number of nucleon resonances with arbitrary spin and space parity) the scalar amplitudes remain real functions of s. On the other hand, such additional mechanisms to the IA, as those described in Ref.[13] lead unavoidably to complex amplitudes for this reaction.

Any polarization observable can be calculated in terms of these scalar amplitudes. In particular, the observables mentioned above can be expressed via the following combinations of them:

$$T_{20} = -\sqrt{2} \frac{-|g_1|^2 + |g_2|^2 + |g_3|^2 - |g_4|^2}{D^2},$$
 (5)

$$\kappa_0 = \frac{3\text{Re} \left[g_3 \cdot \left(g_1 + g_2 + g_4\right)^*\right]}{D^2},$$

$$D^2 = 2 |g_1|^2 + |g_2|^2 + 4 |g_3|^2 + 2 |g_4|^2.$$
(6)

In the IA approach, when the deuteron is considered to contain two nucleons in S- and D-states, only two real independent amplitudes are sufficient to describe the  $dp \rightarrow pd$  process. In this case we have [5]

$$g_4 = g_1,$$
  $g_3^2 = g_1 \cdot g_2,$   
 $g_1 = a^2,$   $g_2 = a^2 \cdot x^2,$  (7)  
 $D = (2g_1 + g_2) = a^2 (x^2 + 2),$ 

where a and x are defined in (1).

But as is shown in the previous section, this approach breaks clown at smaller s than one expects a 6-q description of the deuteron to come into the picture.

A number of more complicated deuteron models and more complicated reaction mechanisms could pretend to explain the revealed effects. In terms of general approach, the next natural step must be an attempt to describe this process by four but sitll real amplitudes. This approach can be justified in generalized version of the IA with the deuteron as superposition with additional P-states (Fig.1b). Such components are inevitable when a relativistic description of the deuteron [14] is used: they also emerge in models based on quark counting [15], when the 6-q states are projected on two-nucleon systems such as NN\*. In this case the process is described by the same diagram as in Fig.1a, with neutron replaced by an N\*.

If the assumption about reality of amplitudes is valid, only 3 independent polarization observables must be measured to reconstruct all of them.

#### 4. What to Measure

New polarization observables can be obtained using a polarized proton target. The simplest polarization observable in this case is the asymmetry of the cross section due to mutual spin orientation of initial protons and deuterons. Here we mention the expressions for transversal spin correlation effect in general case

$$A_{t} = \frac{2\text{Re}\left[g_{3} \cdot (g_{1} + g_{2} - g_{4})^{*}\right]}{D^{2}}$$
 (8)

and (using simplification (7)) in the ONE approach:

$$A_{t} = \frac{2}{9} \frac{u^{4} - 2w^{4} + 3u^{2}w^{2} - uw(5u^{2} - 2w^{2})/\sqrt{2}}{(u^{2} + w^{2})^{2}} = \frac{2x^{3}}{(x^{2} + 2)^{2}}.$$
 (9)

The case with additional *P*-waves is considered in detail in Ref. [5]. As is seen from Fig.5, the new observable is very sensitive to the contribution of possible *P*-states in the deuteron.

The combined analysis of new observable,  $A_t$ , together with those measured earlier, will allow one to reconstruct all amplitudes of the  $dp \rightarrow pd$  process if they are purely real.

We mention for reference that another polarization observable, polarization transfer from the deuteron to the deuteron, is proposed to be measured by a Virginia-Japan-Saclay-Dubna collaboration at KEK (spokesman is C.F.Perdrisat). The general expression for this observable is

$$K_{y,0}^{y',0} = \frac{2\text{Re} (g_1 g_2 + |g_3|^2)}{D^2}.$$
 (10)

One can see that it is a new independent polarization observable. In the ONE approach we have

$$K_{y,0}^{y',0} = \frac{2}{3} \left( \frac{u^2 - w^2 - uw/\sqrt{2}}{u^2 + w^2} \right)^2 = \frac{4x^2}{(x^2 + 2)^2} . \tag{11}$$

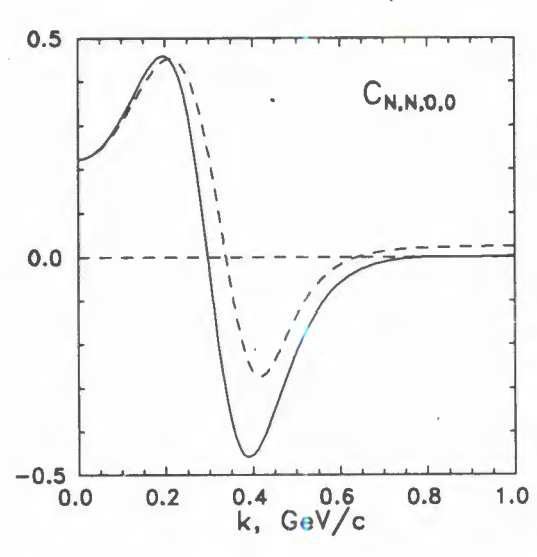


Fig. 5. Spin correlation parameter  $C_{N,N,0,0}$  calculated for standard DWF [11] (solid line) and for DWF with additional P-wave components [14] (dashed line)

Comparing latter expression with (2) it is easy to see that in the ONE approach there is simple relation between expressions for polarization transfer coefficients to the proton and to the deuteron:

$$K_{\nu,0}^{\nu',0} = \frac{4}{9} \kappa_0^2$$
 (12)

As is mentioned above, only additional to IA mechanisms of the reaction generate non-zero imaginary parts in the amplitudes describing this process. All of the polarization observables mentioned above contain combinations of the amplitudes such as  $|g_i|^2$  and/or Re  $(g_i g_k^*)$ . Assuming that the imaginary parts remain small, then they play a role in second order only. In this case any essential deviation from predictions can be interpreted as a non-adequateness of the deuteron model rather than of the reaction mechanism.

To be more sensitive to imaginary parts of the amplitudes it is necessary to measure polarization observables containing the Im  $(g_i g_k^*)$  contributions. Needed combinations appear for only T-odd combinations of the particle polarization vectors and the unit vector along the beam direction (all observables, mentioned above, are T-even).

Here we followed to denotations accepted in Ref. [5]. More accepted denotation for observable suggested to be measured is  $C_{N,N,0,0} = A_t$ .

#### 5. How to Measure

We are planning to measure spin correlation parameter  $C_{N,N,0,0}$  using the Synchrophasotron (Nuclotron) polarized deuteron beam and the Moveable Polarized Target which now is installed at Dubna.

There are two possible ways to select events for BES. Having 180° scattering in the CM system, in Lab system both the final deuteron and the proton go in the forward direction. So, we can select either fast protons or slow deuterons. Our group have an experience in measuring  $T_{20}$  in BES selecting protons. Even having momentum resolution as good as  $\Delta p/p \simeq 0.2\%$  we had the very hard situation to separate elastic events from the

$$d + p \rightarrow p + (n + p)$$

reaction with a small excitation of the (n + p) system comparing with the deuteron mass (Fig.6).

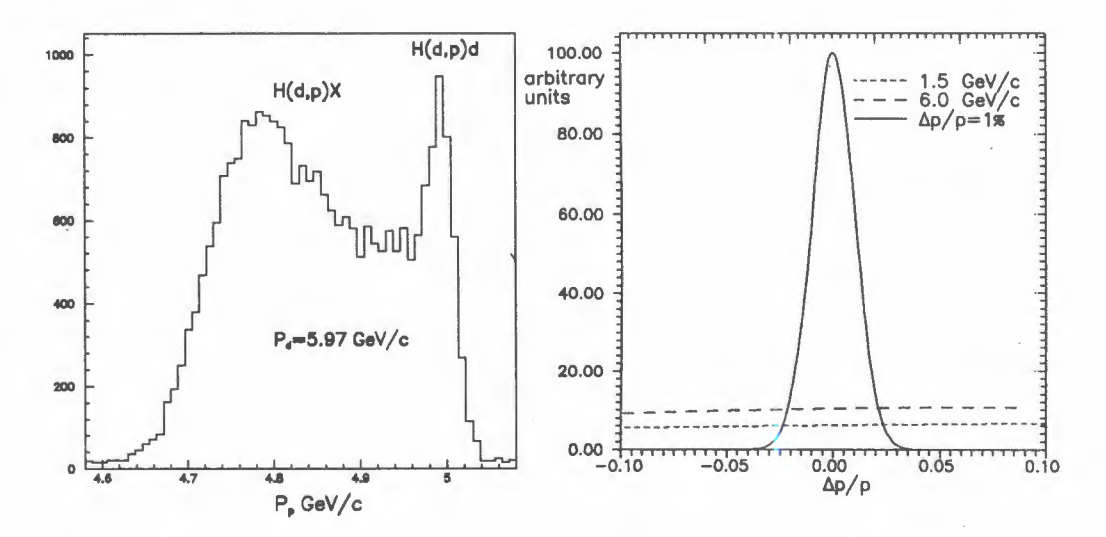


Fig.6. The momentum distributions of protons in Lab system

Fig.7. Contributions of quasi-elastic process on nucleon of the target at the primary beam momentum of 1.5 and 6.0 GeV/c

In case of the MPT the situation will be worse, because the target material contains only  $\simeq 15\%$  of hydrogen: the backward quasi-elastic scattering on the other nuclei in the target will increase the background under the elastic peak considerably.

Selecting of slow deuterons (which we are choosing), gives us the following

advantages:

• no problem to distinguish the deuteron from (n + p) system;

momentum resolution 

1% is sufficient to have a good suppression of quasi-elastic events (see Fig.7);

no problem to distinguish BES from d + p → p + d + π reaction: in latter case the deuteron momentum will be larger (depending on the primary beam energy) as much as 5%—15% (because of opposite directions of the secondary deuteron momentum in the CM and Lab systems, it increases in the Lab while decreasing in the CM).

Unfortunately, we will have disadvantages also. The unfavourable Jacobian (depending on energy 10—30 times worse than in case of selecting of protons) necessitates a large acceptance spectrometer not very far from the target. As a consequence, the space separation between the secondary zero angle deuterons and the primary beam using dipoles is more difficult.

The suggested scheme of the experiment is shown in Fig.8. The last chambers have  $1.4 \times 1~\text{m}^2$  and are situated at the distance of 10 m from the target. The solid angle is  $10^{-2}$  rad. That is 25 times larger than the solid angle for protons during our measurements of  $T_{20}$  [9] and it almost compensates for the unfavourable Jacobian. So, we can evaluate beam time necessary for this experiment from our experience with measurements of  $T_{20}$  at Dubna.

The first stage of separation of the primary and secondary beams will take place in the holding magnet of the MPT. The SP-57 dipole will be used for second stage of separation and the SP-40 dipole will be used both as separating and analysing magnet.

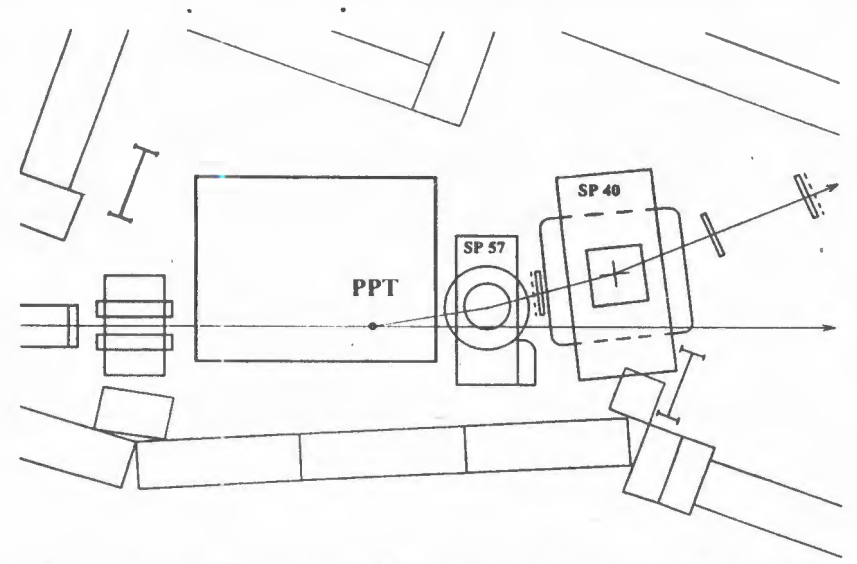


Fig. 8. Layout of the spectrometer. PPT — polarized proton target; SP-57, SP-40 — dipoles; boxes — blocks of proportional chambers; dashed lines — TOF hodoscopes

The distance of about 3 m between proportional chambers downstream and one chamber  $0.3 \times 0.3 \text{ m}^2$  upstream the SP-40 dipole will allow reconstruction of the deuteron momentum with an accuracy of 1% (we assume  $\simeq 100 \text{ mrad bending}$  angle and the accuracy of track detection with proportional chambers of 0.5 mm).

We intend to investigate BES in the region of primary beam of 2.0-6.5 GeV/c. This corresponds to internal momenta of 0.33-0.85 GeV/c will be covered. The secondary deuterons will have momenta of 0.55-1.1 GeV/c. One can see that the ratio between momenta of primary and secondary beams changes from  $\simeq 3$  at lowest energy up to  $\simeq 6$  at highest one. The main task will be to adjust the currents in the dipoles in such a way as to bring the primary beam into a rather narrow gap between the pole and the yoke of the SP-40 dipole. The trajectory of the secondary deuteron beam will change depending on the energy of the primary beam. So, the system of proportional chambers must be moveable in a direction transversal to the beam.

The deuterons of interest will be accompanied by huge background, mostly pions and protons of the same momenta; therefore we need to have a high resolution time of flight (TOF) system. Besides, we expect high flux (especially through the first chamber) of forward elastically scattered deuterons and of protons of half of the primary beam momentum. There will be no problem to distinguish such events from the desired ones, but too high flux of other particles will require the following measures:

instead of simple TOF counters overlapping proportional chambers we need to install
two hodoscopes. In this case we will have rough position of tracks due to the hodoscopes which will prompt us to choose relevant tracks in proportional chambers
where we expect as a rule many tracks situation;

unambiguous identification of the good track in the first and last blocks of proportional chambers (thanks to hodoscopes) and condition of straight line in the y-plane will help us find the relevant tracks in the first chamber block downstream of the magnet.

#### 6. Conclusion

The analysis of polarization observables such as  $T_{20}$  and polarization transfer coefficient both in the p(d, p) d and A(d, p) X (zero angle) reactions obtained at Saclay and Dubna shows deviation from the IA based on a DWF with S-D-components only. New independent polarization characteristics must be measured to check whether we are dealing with more complex reaction mechanisms or with more than two-component DWF.

We suggest here to measure new polarization observable for the backward elastic dp scattering, namely, the spin correlation parameter, when both initial deuteron and proton have the transversal (parallel or antiparallel) polarization. Such an observable of this reaction has never been measured. Firstly this observable was considered in Ref. [5] where it is shown that this observable is most sensitive to any deviations of the deuteron structure from the commonly accepted picture, in particular, respectively possible existing of P-wave. Such measurements are an important step in the realization of the complete experiment for this reaction.

The internal momentum region of 0.33-0.85 GeV/c will be covered, when changing the primary beam momentum from 2.0 up to 6.5 GeV/c. We intend to measure 10 points inside pointed out region with the error bars about  $\pm 0.03$ . The beam times request is about 15 days (for data taking only).

A total of about 300,000\$ is needed to assemble a spectrometer for this experiment; this spectrometer can also be used for other experiments using polarized target in the future [16,17].

#### 7. Acknowledgements

This work is supported in part by Russian Foundation for Fundamental Researches, grant № 93-02-3961, № 95-02-0504.

The authors would like to express their thankfulness to A.M.Baldin, J.Arvieus, V.G.Kadyshevsky, F.Lehar, A.N.Sissakian for strong support of this activity.

They are grateful to N.Angelov, I.Atanasov, V.A.Bodyagin, J.Durand, A.P.Dzyubak, A.V.Efremov, M.Finger, V.V.Glagolev, L.B.Golovanov, F.Gross, T.Hasegawa, V.A.Karmanov, B.A.Khachaturov, A.D.Kovalenko, N.B.Ladygina, A. de Lesquen, Ph.Leconte, S.Nedev, V.G.Neudachin, I.T.Obukhovsky, L.Penchev, V.Penev, I.L.Pisarev, A.N.Prokofiev, P.A.Rukoyatkin, M.G.Sapozhnikov, L.A.Sarycheva, P.V.Sorokin, H.Spinka, G.D.Stoletov, E.A.Strokovsky, J.J. de Swart, E.Tomasi-Gustafsson, M.Tokarev, Yu.A.Usov, V.V.Vihrov, L.Vizireva, H.J.Weber, A.A.Yershov, A.A.Zhdanov for useful discussions and stimulating interest in the present work.

#### References

- 1. Berthet P. et al. J. Phys. G.: Nucl. Phys., 1982, 8, p.L111.
- 2. Arvieux J. et al. Nucl. Phys., 1984, A431, p.6132.
- 3. Bosted P. et al. Phys. Rev. Lett., 1982, 49, p.1380.
- 4. Kobushkin A.P. J. Phys. G: Nucl. Phys., 1986, 12, p.487.
- 5. Sitnik I.M., Ladygin V.P., Rekalo M.P. Yad. Fiz., 1994, 57, p.1270.
- 6: Vasan S.S. Phys. Rev., 1973, D8, p.4092.
- 7. Kuehn B., Perdrisat C.F., Strokovsky E.A. JINR, E2-94-95, Dubna, 1994, p.31.
- 8. Kobushkin A.P., Syamtomov A.I., Perdrisat C.F., Punjabi V. Phys. Rev., 1994, C50, p.2627.
- Azhgirey L.S. et al. In: Abstracts of 14-th Int. IUPAP Conf. on Few Body Problems in Physics, Willjamsburg, USA, May 26—31, 1994, p.22.
- Punjabi V. et al. In: Abstracts of 14-th Int. IUPAP Conf. on Few Body Problems in Physics, Willjamsburg, USA, May 26—31, 1994, p.161, and to be published in Phys. Lett. B, 1995.
- 11. Lacombe M. et al. Phys. Lett., 1981, B101, p.139.
- 12. Ghazikhanian V. et al. Phys. Rev., 1991, C43, p.1532.
- 13. Kondratyuk L.A., Lev F.M., Schevchenko L.V. Yad. Fiz., 1979, 29, p.1081.
- 14. Buck W.W., Gross F. Phys. Rev., 1979, D20, p.2361.
- 15. Glozman L. Ya., Neudatchin V.G., Obukhovsky I.T. Phys. Rev., 1993, C48, p.389.
- Ellis J., Karliner M., Kharzeev D.E., Sapozhnikov M.G. Preprint CERN-TH.7326/94 (1994).
- 17. Ladygin V.P., Ladygina N.B. JINR Preprint E1-94-279, Dubna, 1994; to be published in Yad. Fiz., 1995.

УДК 539.171.018 + 539.172.138.12

### WHAT SHOULD BE MEASURED IN DEUTERON BREAKUP WITH POLARIZED PROTON TARGET

#### E.A. Strokovsky

At present, two different approaches are used for interpretation of inclusive data on deuteron breakup with emission of proton-fragments at zero degree by hadrons. According to one of them the observed characteristics of this reaction (cross sections, polarization observables) are determined by the reaction mechanism and the deuteron structure at short distances (in the commonly accepted sense) plays a minor role. According to the other approach it is the deuteron structure at short distances which determines the observed trend of the data. Neither of these approaches can describe the data even qualitatively in the whole investigated region of kinematical variables, having particular success for some narrow region corresponding to long distances. Installation of the polarized proton target at LHE JINR opens an opportunity to perform a rather simple experiment which could discriminate one of these completing approaches. The idea of this experiment is discussed in the present paper. Measurement of the observable suggested here is a particular example of a general problem of a search for spin correlations in inelastic reactions between particles separated well in 4-velocity or rapidity spaces. In our particular case correlations of spin degrees of freedom between particles, one of which is in the target fragmentation region and the other belongs to the projectile fragmentation region, are discussed.

The investigation has been performed at the Laboratory of High Energies, JINR.

### Что следует измерить в реакции инклюзивного развала дейтрона поляризованными протонами

#### Е.А.Строковский

В настоящее время существуют два основных подхода к интерпретации инклюзивных данных о развале дейтрона адронами с вылетом протонов-фрагментов «вперед». Согласно одному из них характеристики этой реакции (сечения и поляризационные наблюдаемые) определяются в первую очередь механизмом реакции, а структура дейтрона на малых расстояниях, понимаемая в общепринятом смысле, играет второстепенную роль. В другом подходе считается, напротив, что именно структура дейтрона на малых расстояниях определяет, в основном, наблюдаемое поведение данных. Ни один из этих подходов не может обеспечить описание данных во всей исследованной области кинематических переменных даже качественно, хотя в обоих достигается неголохое описание данных в некоторой области, отвечающей сравнительно большим расстояниям. Установка поляризованной протонной мишени в ЛВЭ ОИЯИ открывает возможность выполнить сравнительно простой эксперимент, который мог бы дать основу для выбора между этими конкурирующими точками зрения. В данной работе обсуждается идея такого опыта. Измерения наблюдаемой, предложенные в этой работе, представляют собой частный случай общей проблемы поиска корреляций между спинами частиц, хорошо разделенных в пространстве 4-скоростей или быстрот. В частном случае, рассмотренном здесь, обсуждается корреляция между спиновыми степенями свободы частиц, одна из которых принадлежит области фрагментации мишени, а другая — снаряда.

Работа выполнена в Лаборатории высоких энергий ОИЯИ.

#### 1. Why an Additional Polarization Observable is Necessary

Reaction  $d + (p, A) \rightarrow p + X$  of inclusive deuteron breakup when proton is emitted at zero degree with momentum  $p > p_d/2$  is under study about 15 or more years. Here  $p_d$  is the momentum of the initial deuteron. Data of high quality are obtained on differential cross sections [1], tensor analysing power  $T_{20}$  [2] and spin transfer coefficient  $\kappa_0$  from the deuteron to the proton-fragment [3]. The main goal of these efforts was to get information about deuteron structure at short distances where its nucleons-constituents can hardly be treated as separate objects and quark-gluon effects should be revealed. Of course, such kind of information can be obtained from experiments with electromagnetic probes as well; a wide-spread belief is that it is the best way. But use of hadron probes has some advantages before electromagnetic ones; apart from higher cross sections disintegration of deuterons by hadrons is sensitive not only to charged (quark) constituents of deuteron but to its gluonic component as well. The expression «deuteron structure» is used here in a commonly accepted sense, i.e., it can be represented in terms of deuteron structure functions or its wave function, which can be found as a solution of some set of equations with boundary conditions corresponding to the problem of the stable bound system with the deuteron quantum numbers.

Generally speaking, in the experiments mentioned above the polarization observables were measured in the projectile fragmentation region and correlations of spin degrees of freedom between incident deuteron and its proton-fragment were studied when these particles are more-or-less close to each other in the 4-velocity or rapidity spaces, i.e., the close correlations were studied.

The motivation of experiments on hadro-disintegration of deuteron is based on implicit assumption that the matrix element of this reaction can be factorized on two parts: the one part is determined by deuteron wave function (DWF), the other one describes interaction of the deuteron constituents with target, i.e., represents a particular reaction mechanism. The assumption, or a belief we are talking about, is that the 2nd part of the matrix element, i.e., a particular mechanism of the breakup reaction, has comparatively weak influence on the behaviour of the measurable quantities (the cross sections, polarization observables) which are determined mostly by the DWF. This assumption can be expressed in other words as an assumption of absence of significant spin correlations between target and projectile fragmentation regions when 4-velocity or rapidity spaces are considered. There are evidences in favor of this (see, for examples, Refs. [4,5]). Still, this is not proven neither experimentally nor theoretically so far. Therefore there is no commonly accepted interpretation of the data mentioned above.

According to one point of view, the discrepancies between the data and theoretical model calculations [5] are a signal about necessity to make various modifications of the DWF, according to the others [6], it is the reaction mechanism which is responsible for these discrepancies.

Recently it was shown, that if the DWF has commonly accepted 2-component structure with S and D waves at distances where nucleons can be treated as the separate entities, and

if the reaction mechanism does not change the spin state of the detected protons, then the two polarization observables,  $T_{20}$  and  $\kappa_0$  must be related and fill a circle on the  $T_{20}-\kappa_0$  plane [7]. The experimental data show that it is not so: at least one of these conditions is not fulfilled [4, 7]. The present state of theory and the experimental data base cannot provide a basis for a definite conclusion which of two possible reasons is responsible for the deviation of the experimental data from theoretical expectations.

In all the experiments on the hadrodisintegration performed so far only unpo $d \xrightarrow{A} X$ 

Fig. Inclusive breakup of deuteron in IA-like approximation

larized targets were used. We would like to stress here that the breakup of unpolarized deuterons on *polarized protons* can help much in finding of *definite conclusion* about the relative importance of the reaction mechanism.

Indeed, if one takes the assumption that the reaction mechanism does not change the spin state of the detected proton, i.e., this state is determined by its spin state in the deuteron before it was broken (at distances where it has a sense to talk about spin state of proton in deuteron), then the polarization of protons  $P_p$  from breakup of unpolarized deuterons on polarized target must be zero. It is evident from the simplest IA-like graph of the Figure widely used for interpretation of the breakup data. In other words: there must be no correlation between  $P_p$  and polarization  $P_t$  of the target, i.e., between spin degrees of freedom when one considers particles separated far in the 4-velocity or rapidity spaces. This correlation parameter is denoted here as  $K_{0,y}^y$  where lower indices refer to the initial particles (projectile and target) and upper index refers to the detected particle; this notation is constructed in analogy with notations used in Ref. [8] where elastic backward deuteron-proton scattering (BES) was analysed.

On the other hand, if the reaction mechanism does change the spin state of the detected proton, then there could be sizeable correlation between  $P_p$  and  $P_t$ . This is evident, for example, if configurations with at least 3 nucleons (2 from deuteron + 1 from target) with relative distances less than ~0.5 Fm in the coordinate space play significant role in the process of the deuteron breakup with emission of a hard proton with momentum  $p > p_d/2$ .

Therefore the measurement of the spin transfer from polarized proton target to the proton-fragment, i.e.,  $K_{0,y}^y$  in breakup of unpolarized deuterons could give an almost definite answer to the key questions: what we are studying in the deuteron breakup: a mechanism of this reaction or the deuteron structure (if they can incleed be disentangled and this question makes sense).

#### 2. Some Details of the Experiment

The experiment can be performed at LHE JINR using Moveable Polarized Proton Target which has been installed in the Laboratory.

In order to reach the main goal formulated above it would be enough to measure  $K_{0,y}^y$  up to k of 300—400 MeV/c, where large discrepancies are observed between data and almost all theoretical models. Here k is the light-cone variable (see [1, 2, 3, 5] for example). In this kinematical region the breakup cross sections are rather big [1] and problem of particle identification is not so difficult as it was in the previous experiments [2, 3], where data were taken at k close to the kinematical limit.

Because of low content of polarized protons in the target working material used now, it would be better to replace it by irradiated NH<sub>3</sub> which has two main advantages for this experiment:

- all the scattering centers are polarized because the nitrogen nuclei are polarizable as well as protons;
- the upper acceptable level of intensity of the primary beam is much higher with irradiated ammonia.

Another advantage of measuring  $K_{0,y}^y$  in this experiment (as well as  $K_{0,y}^{0,y}$  in BES) in comparison with measurements of  $\kappa_0$  or spin-spin correlation  $C_{y,y}$  in the deuteron breakup or BES [9] is that intensity of unpolarized deuteron beam at the Synchrophasotron or the Nuclotron is much higher than the intensity of polarized deuteron beam. Therefore the data taking rates will be limited by the setup capacity only.

The magnetic spectrometer with momentum resolution of ~0.3—0.5% placed down-stream the target must include a proton polarimeter like the POMME polarimeter [10] working at SATURNE or a new polarimeter to be built at LHE.

#### 3. Conclusion

Measurement of the spin transfer coefficient  $K_{0,y}^y$  from polarized proton target to the hard proton-fragment in reaction of inclusive deuteron breakup at zero degree is suggested to be performed at the extracted beam of unpolarized deuterons of the Synchrophasotron or the Nuclotron. If this coefficient will be small and close to zero up to  $k \sim 300-400$  MeV/c, it will be a strong experimental argument that the breakup of deuteron by hadrons probes the deuteron structure at short distances. If the coefficient  $K_{0,y}^y$  will deviate significantly from zero at  $k \sim 300-400$  MeV/c, it will be an unambigious argument in favour of alternative approaches like those where reaction mechanism contains strong final state interaction and intermediate isobars and mesons play a decisive role or those where some system of 9 quarks or 3 correlated nucleons appears in the intermediate state.

Of course, other possible spin observables should be examined (first of all theoretically) as well: the coefficient of tensor-to-vector spin transfer from tensorially polarized deuteron to proton and the triple spin correlations (polarized deuteron, polarized target

proton and polarized final proton-fragment). Some of them could be unsignificant within IA-like models where graphs like on the Figure are dominant, but could be essentially non-zero in alternative approaches.

In our particular case a particular correlation of spin degrees of freedom between particles belogning to target and projectile fragmentation regions was discussed. In this sense the measurements of observable suggested here give a particular example of more general problem of a search for spin correlations in inelastic reactions between particles separated well in 4-velocity or rapidity spaces.

#### Acknowledgments

The author is grateful to A.P.Kobushkin for his stimulating interest and useful discussions of the topics considered in this paper.

The work was financially supported in part by grant №RFU000 of the International Science Foundation.

#### References

Ableev V.G. et al. — Pis'ma ZhETF, 1983, 37, p.196; Nucl. Phys., 1983, A393, p.491, A411, 541 (E); Pis'ma ZhETF, 1987, 45, p.467; JINR Rapid Comm. 1[52]-92, Dubna, 1992, 10; Few Body Systems, 1990, 8, p.137;

Perdrisat C.F. et al. - Phys. Rev. Lett., 1987, 59, p.2840;

Punjabi V. et al. — Phys. Rev., 1989, C39, p.608.

- Punjabi V. et al. Phys. Rev., 1989, C39, p.608;
   Ableev V.G. et al. —Pis'ma ZhETF, 1988, 47, p.558; JINR Rapid Comm. 4[43]-90, Dubna, 1990, p.5.
- Cheung E et al. Phys. Lett., 1992, B284, p.210;
   Atanasov I et al. Proc. of the 10-th Internat. Symp. on High Energy Spin Physics, Nov. 9—14, 1992, Nagoya, ed. by Hasegawa T., Horikawa H., Masaike A., Sawada S., Univ. Acad. Press, Inc., Tokyo, p.537;
   Kuehn B. et al. Phys. Lett., 1994, B334, p.298;

Nomofilov A.A. et al. — Phys. Lett., 1994, B325, p.327.

- 4. Azhgirey L.S. et al. 14th Intern. IUPAP Conf. on Few Body Problems in Phys., May 26—31, 1994, ed. by Franz Gross, Williamsburg, 1994, p.18; ibid p.22; and references therein; see also Refs [5, 7].
- 5. Kobushkin A.P., Shelest V.P. Physics of Elementary Particles and Atomic Nuclei, 1983, 14, p.1146;

Kobushkin A.P. — Proceedings of the International Symposium «Dubna — Deuteron-93», Dubna, Sept. 14—18, 1993, JINR, E2-94-95, Dubna, 1994, p.71;

Perdrisat C.F., Punjabi V. — Phys. Rev., 1990, C42, p.608;

Kobushkin A.P. — J. Phys. G: Nucl. Phys., 1986, 12, p.487;

- Perdrisat C.F., Punjabi V. Proceedings of the XI Internat. Seminar on High Energy Physics Problems, Sept. 7—12 1992, Dubna, p.491, ed. by Baldin A.M., Burov V.V., Dubna, 1994.
- Lykasov G.I., Dolidze M.G. Z. Phys., 1990, A336, p.339;
   Lykasov G.I. Physics of Elementary Particles and Atomic Nuclei, 1993, 24, p.140;
   Dorodnykh Yu.L., Lykasov G.I. Proceedings of the International Symposium «Dubna Deuteron-93», Dubna, Sept. 14—18, 1993, JINR, E2-94-95, Dubna, 1994, p.83.
- Kuehn B., Perdrisat C., Strokovsky E.A. Proceedings of the International Symposium «Dubna Deuteron-93», Dubna, Sept. 14—18, 1993, JINR, E2-94-95, Dubna, 1994, p.31; JINR Preprint E1-95-7, Dubna, 1995.
- 8. Kobushkin A.P. et al. Phys. Rev., 1994, C50, p.2627.
- 9. Sitnik I.M., Ladygin V.P., Rekalo M.P. Yad. Fiz., 1994, 57, p.2170.
- 10. Bonin B. et al. NIM in Phys. Rev., 1990, A228, p.379.

УДК 539.125.4 539.12...162.8

### AN EVIDENCE FOR COLLECTIVE PHENOMENON IN HEAVY ION COLLISIONS AT 4.2 A GeV/c

A.P. Cheplakov, A.A. Kuznetsov, R.R. Mekhdiyev<sup>1</sup>, M.I. Soloviev Joint Institute for Nuclear Research, Dubna, 141980, Russia

L.M.Shcheglova, A.N.Solomin

Nuclear Physics Institue, Moscow State University, Moscow, 119899, Russia

S. Backović, D. Salihagić

University of Montenegro, Podgorica, 81000, Montenegro, Yugoslavia

Recent data on  $^{12}C + ^{12}C$  and  $^{12}C + ^{181}Ta$  interactions at 4.2 A GeV/c from the 2 m JINR propane bubble chamber exposed at the Dubna Synchrophasotron are presented. The analysis of the flow angle distributions shows the «side-splash» effect in reactions with tantalum and carbon targets for high multiplicity events though for the latter case it is rnuch less pronounced.

The investigation has been performed at the Particle Physics Laboratory and Laboratory of High Energies, JINR.

#### Наблюдение коллективных потоков в соударениях тяжелых ионов при 4.2 *A* ГэВ/с

#### А.П.Чеплаков и др.

Представлены данные по взаимодействиям <sup>12</sup>C + <sup>12</sup>C и <sup>12</sup>C + <sup>181</sup>Та при 4.2 А ГэВ/с, полученные при облучении двухметровой пропановой пузырьковой камеры на синхрофазотроне ЛВЭ ОИЯИ. Анализ распределений по углу потока показывает наличие «sidesplash» эффекта в соударениях с танталовой и углеродной мишенями в событиях с большой множественностью. В то же время эффект для углеродной мишени выражен менее заметно.

Работа выполнена в Лаборатории сверхвысоких энергий и Лаборатории высоких энергий ОИЯИ.

#### 1. Introduction

High energy nucleus-nucleus interactions have been of growing interest in the recent years. This is mainly due to the fact that these collisions offer a unique opportunity to study properties of nuclear matter at extremely high densities and temperatures, where the phase

<sup>&</sup>lt;sup>1</sup>On leave of absence from Institute of Physics, Azerbaijan Academy of Sciences, 370143 Baku, Azerbaijan

transition of hadron gas to quark-gluon plasma and other novel phenomena may exist. In this context the main features of particle production and general properties of the intranuclear medium are to be studied covering both low and high energy regions in order not to miss a signal of exotics.

One of the most significant experimental results in this field was the observation of the collective flow of nuclear matter in the region of relatively low energies (around 1 GeV per nucleon) which was considered as the most important signature for the compression effects proposed by an equation of state. In the experiments with Plastic Ball [1] and later on with the streamer chamber [2] (both at the BEVALAC, Berkeley) the existence of the twofold collective effect was established: the «side-splash» of the participants and the «bounce-off» in the fragmentation region. Further investigations in the energy range around 1 GeV have confirmed the effect [3—5]. At higher energies (about a few GeV per nucleon) nuclei still exhibit a rather large stopping power [6], and so the collective flow might well exist in this energy region and its nature should be similar to that at low energies. However there was no experimental evidence for (or against) the stopping power [6], and so the collective flow might well exist in this energy region and its nature should be similar to that at low energies. However there was no experimental evidence for (or against) the existence of nucleonic collective flows at medium energies.

We searched for a possible manifestation of the nontrivial collective phenomena in collisions of carbon nuclei with carbon and tantalum ones at 4.2 GeV/c per nucleon. The experimental results are compared with the Monte-Carlo calculations according to the Dubna version of the cascade model (DCM) [7].

#### 2. Experimental Details

The experiment was carried out with the 2 m propane bubble chamber exposed to the beams of d,  $^4$ He and  $^{12}C$  nuclei at the incident momentum of 4.2 GeV/c per nucleon from the Dubna Synchrophasotron. Three tantalum plates each 1 mm thick were placed inside the chamber volume. Events were recorded in the target plates as well as in propane. The statistics is ~2000 for  $^{12}C + ^{181}Ta$  interactions and ~7000 for the  $^{12}C + ^{12}C$  case. Protons were well separated from pions in the momentum range of  $150 MeV/c by ionization density. The contamination of misidentified <math>\pi^+$  mesons was about 8% of the number of fast positively charged particles with p > 1 GeV/c which were mainly fast protons [8]. The charges of fragments heavier than proton were determined by ionization density and also by means of counting  $\delta$  electrons in the case of carbon exposure [9]. The contamination of such fragments was about 7% of the number pf positive tracks in the momentum range from 1 to 2 GeV/c [8]. The experimental setup and the data handling procedure are described in more detail in refs. [10—12].

For the analysis presented below we used the number of participant protons, i.e., protons which took part in the interaction, defined as

$$N_{\text{part}} = n_{c} - n_{\pi^{-}} - n_{\pi^{+}} - n_{P}^{F} - n_{T}^{F}, \tag{1}$$

where  $n_c$  is the number of charged particles in an event,  $n_{\pi^-}(n_{\pi^+})$  is the number of  $\pi^-(\pi^+)$  mesons and  $n_P^F(n_T^F)$  is the number of spectator fragments of the projectile nucleus (target nucleus). The value of  $n_T^F$  is determined by the number of spectator fragments of the projectile (or stripping particles) with p/Z > 3 GeV/c and with the emission angle < 4°. Protons with  $p_{\rm lab} < 450$  MeV/c were considered as spectator fragments of the target the most part of which was absorbed by the tantalum plate. This boundary obtained in a special methodic analysis is rather nominal, however the charge of its absolute value within the limits of reasonable physical estimates does not affect the results of the experimental analysis presented below.

For the sake of proper comparison of the DCM predictions with the data, we have filtered the simulated events through the program which imitates the main features of the whole chain of the data taking and processing procedures. A good agreement of the inclusive single-particle spectra from simulated events with the data is a combined success of both the DCM and the filtering [8].

## 3. Event Shape Analysis and Collective Flow

Search for experimental evidence of collective effects in our experiment has been carried out by means of the events shape analysis based on the diagonalization of the kinetic energy flow tensor [13].

$$K_{ij} = \sum_{\mathbf{v}} \frac{p_i(\mathbf{v})p_j(\mathbf{v})}{2m(\mathbf{v})} . \tag{2}$$

This sphericity tensor with the weight factor 1/2m(v) was determined and diagonalized for each individual event. For C+C collisions this procedure was performed in the center-of-mass system while for asymmetric C+Ta collisions we used two different reference frames as described below. In the event shape analysis we also used the flow angle,  $\theta_{FL}$ , as a key variable. It is defined as the angle between the beam axis and the major axis of the flow ellipsoid obtained after the diagonalization of the  $K_{ij}$  tensor. In order to reveal the nontrivial collective nucleons flow (the «side-splash» effect), the  $\theta_{FL}$  distributions for C+Ta and C+C collisions were obtained for different multiplicity selections, and the comparison with those calculated from the DCM was made.

The distributions of the flow angle  $\theta_{FL}$  in the nucleon-nucleon center-of-mass system (NN c.s.s.) for all protons produced in C+Ta interactions at 4.2 GeV/c per nucleon for different intervals of multiplicity  $n_c$  are shown in Fig.1 (a). The corresponding distributions obtained from the DCM-simulated and appropriately filtered events are also presented on the right of this picture (Fig.1 (b)). As is seen from Fig.1 (a), the  $\theta_{FL}$  distributions for all protons (spectators and participants) do not show any peculiarities at nonzero  $\theta_{FL}$ , i.e., we do not see any «side-splash» of protons. Similarly the DCM also produces smooth distributions.

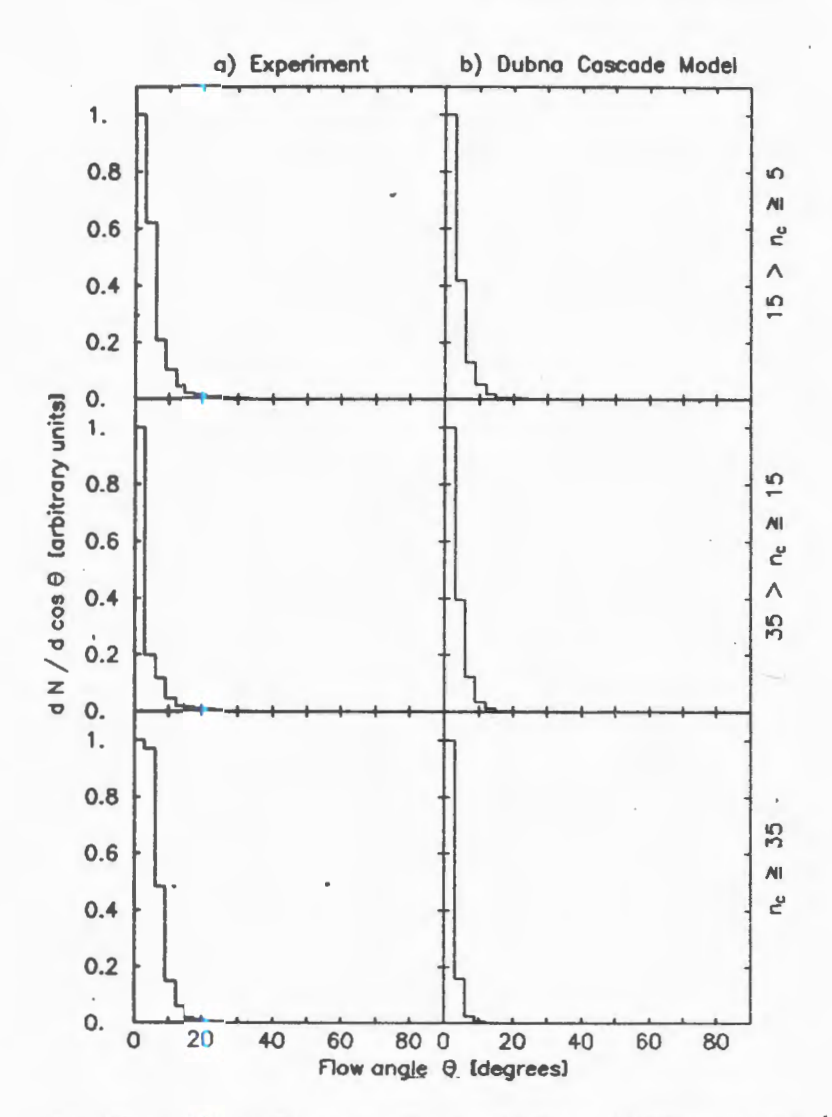


Fig.1. Flow angle distributions for C+Ta collisions in different multiplicity intervals for all protons in the NN c.m.s.

It should be noted here that as the data presented in Fig.1 (a) include also the spectators, the sidewards flow can be seen only if it is significant enough since the effect must be masked by spectator protons from the projectile which are mainly peaked at small angles  $(\theta_{FL} < 10^{\circ})$ . This has been realized previously in the experiments at the BEVALAC [1,2]. Another point is that the NN c.m.s. is not quite meaningful when the masses of the colliding nuclei are not equal. Much closer to the proper c.m.s. of the interacting matter is the center-of-mass system of participant nucleons (p.c.m.s), in which  $\sum p_{\text{long}}^*(v) = 0$ , where v

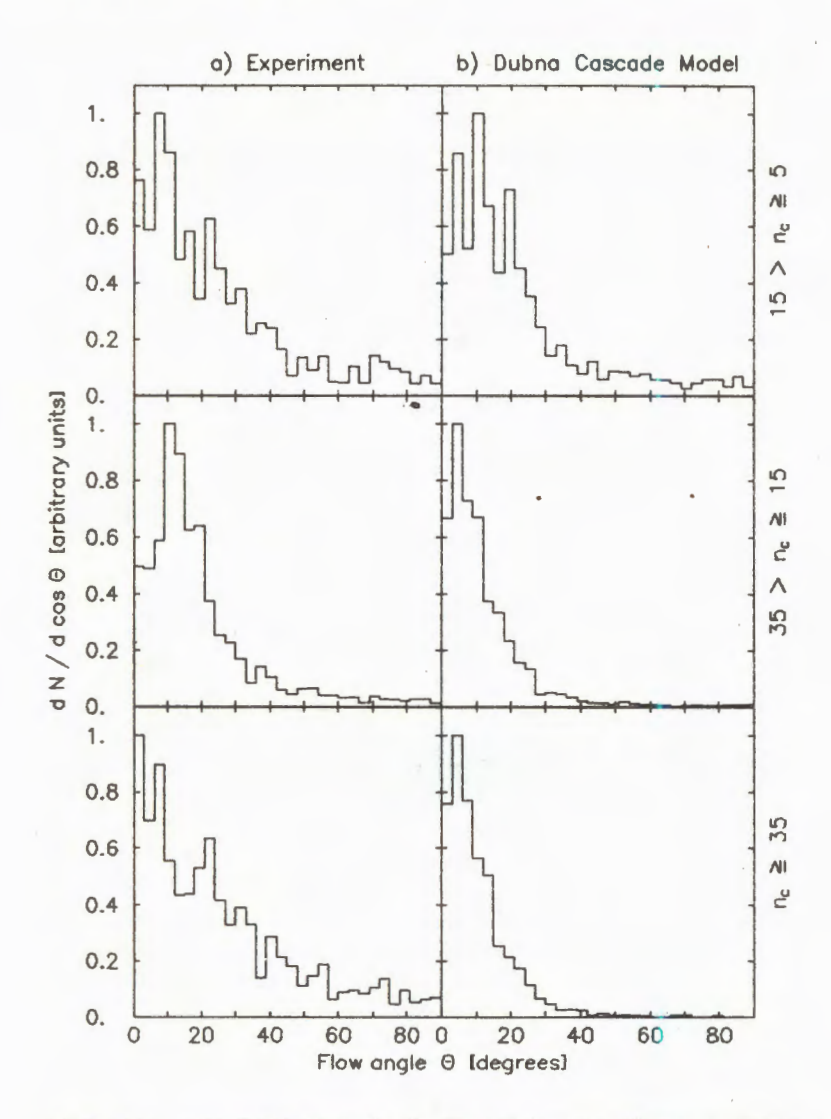


Fig. 2. Flow angle distributions for C+Ta collisions in different multiplicity intervals for participant protons in their center-of-mass system

runs over the participant nucleons. Thus, in order to reveal a signal of collective «side-splash» (if any), we have also obtained the  $\theta_{FL}$  distributions for participant protons in the p.c.m.s., i.e., in their own rest system. From the distributions presented in Fig.2 (a) it is seen that there is a distinct peak near  $\theta_{FL} \sim 12^{\circ}$  for the  $15 \le n_c < 35$  charged multiplicity bin. The distributions obtained from the DCM, which does not comprise collective effects, are also shown in the same figure. These distributions demonstrate a rather smooth fall towards large  $\theta_{FL}$  angles (Fig.2 (b)).

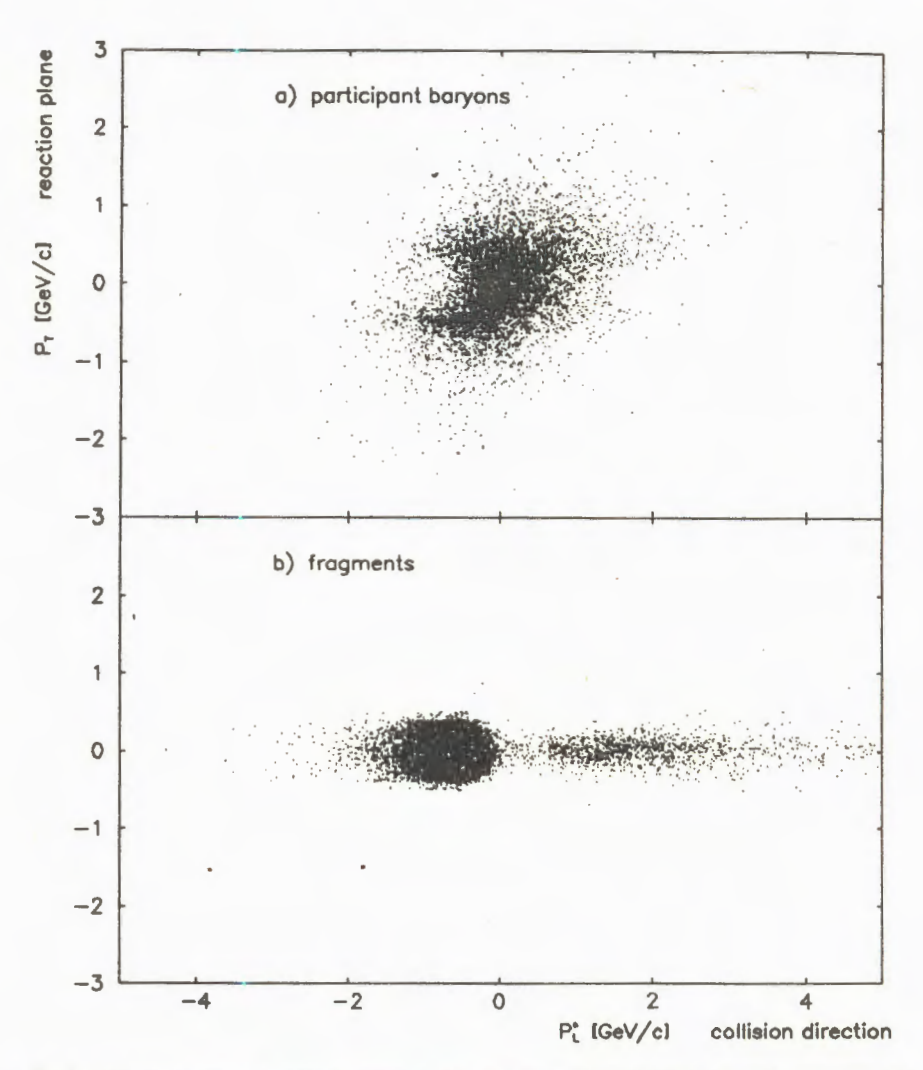


Fig. 3. Projection onto the reaction plane of the momenta of participants (a) and spectators (b) in the c.m.s. of participants (C + Ta data, experiment)

Figure 3 presents an inclusive momentum configuration of participant protons and spectator protons of colliding nuclei for C + Ta interactions. For each event the longitudinal momenta of particles were Lorentz-transformed into the rest frame of participant protons. The plane containing the major axes of the  $K_{ij}$  tensor and the beam axis (reaction plane) was determined for each event and rotated by azimuthal angle  $\varphi$  in such a way that the individual reaction planes coincided with the x-z plane, where the z-axis is the beam one. In other words, the reaction planes were superposed for all events. For better visualization only the particles having small momentum components transversal to the flow plane

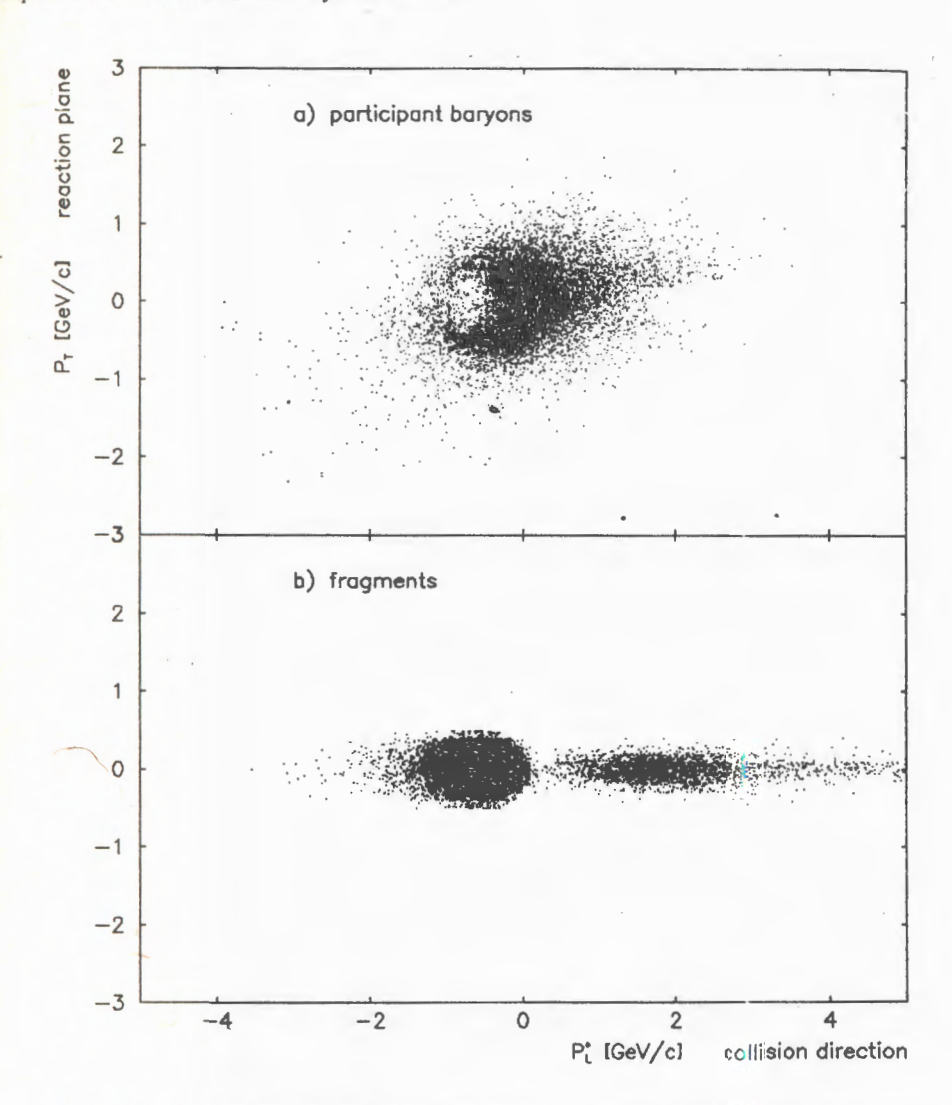


Fig.4. Projection onto the reaction plane of the momenta of participants (a) and spectators (b) in the c.m.s. of participants (C + Ta, DCM calculations)

 $(p_T^{\rm out} < 0.2~{\rm GeV/c})$  are shown. It is seen that our criteria for separation of the spectators work well since we do not observe any significant presence of nucleons from the fragmentation regions of colliding nuclei in Fig.3a. Analogous distributions from the cascade model are presented in Fig.4. The comparison of Figs.3 and 4 shows that the DCM describes qualitatively quite well the dynamics of collision at our energy. So, any significant deviation from the experiment can be considered as a possible signal of a collective phenomenon because there is no collective mechanism input in the DCM.

The above analysis shows that there is a finite deflection angle for a mid-multiplicity interval in C + Ta interactions. The same analysis was made for C + C interactions in our

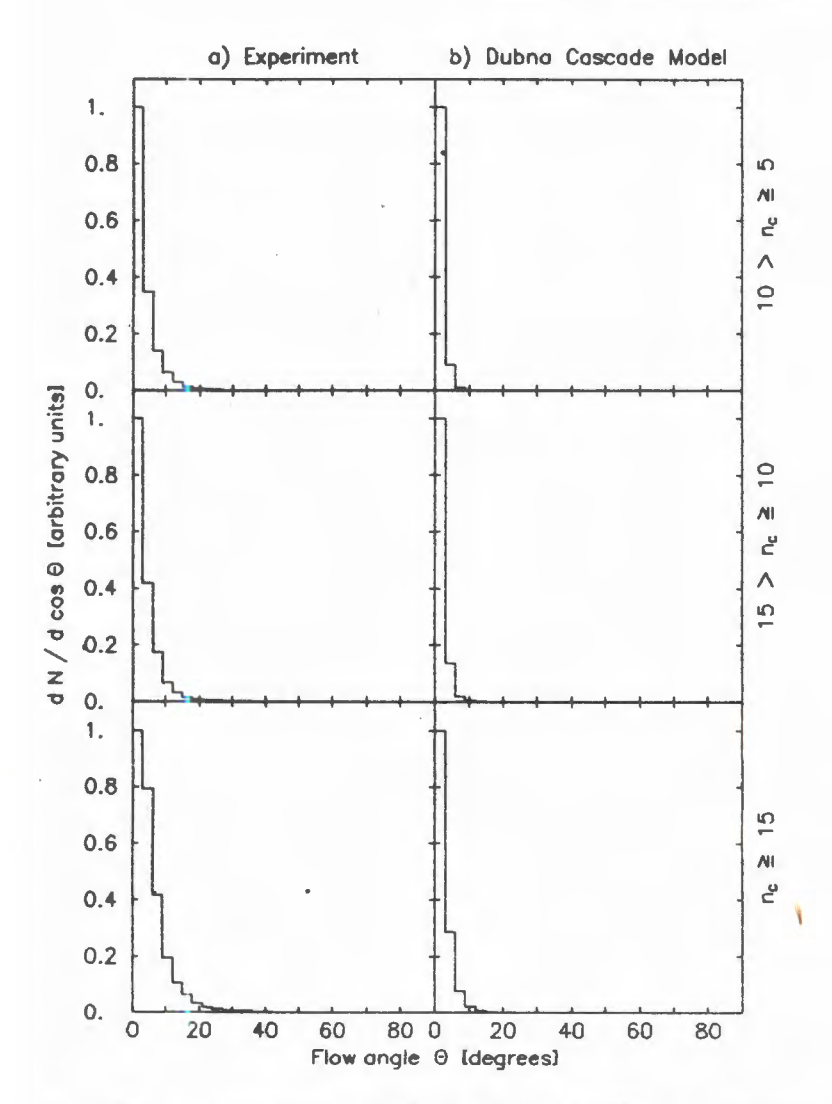


Fig. 5. Flow angle distributions for C + C collisions in different multiplicity intervals for all protons in the c.m.s.

experiment. As in the case of C + Ta interactions, the  $\theta_{FL}$  distributions of all protons in the c.m.s. of colliding nuclei were obtained for interactions of incoming carbon nucleus with carbon from propane (C + C interactions, Fig.5 (a)). Analogous  $\theta_{FL}$  distributions of filtered events from DCM calculations are presented in the same figure (Fig.5 (b)). There is no structure seen in Figs.5 (a,b): the  $\theta_{FL}$  distributions are smooth and fall down steeply. The flow angle distributions for C + C data, where only participant protons were included in the analysis, along with the DCM calculations are shown in Figs.6 (a,b). As is seen from Fig.6, the comparison of the experimental data with the cascade model calculations shows the

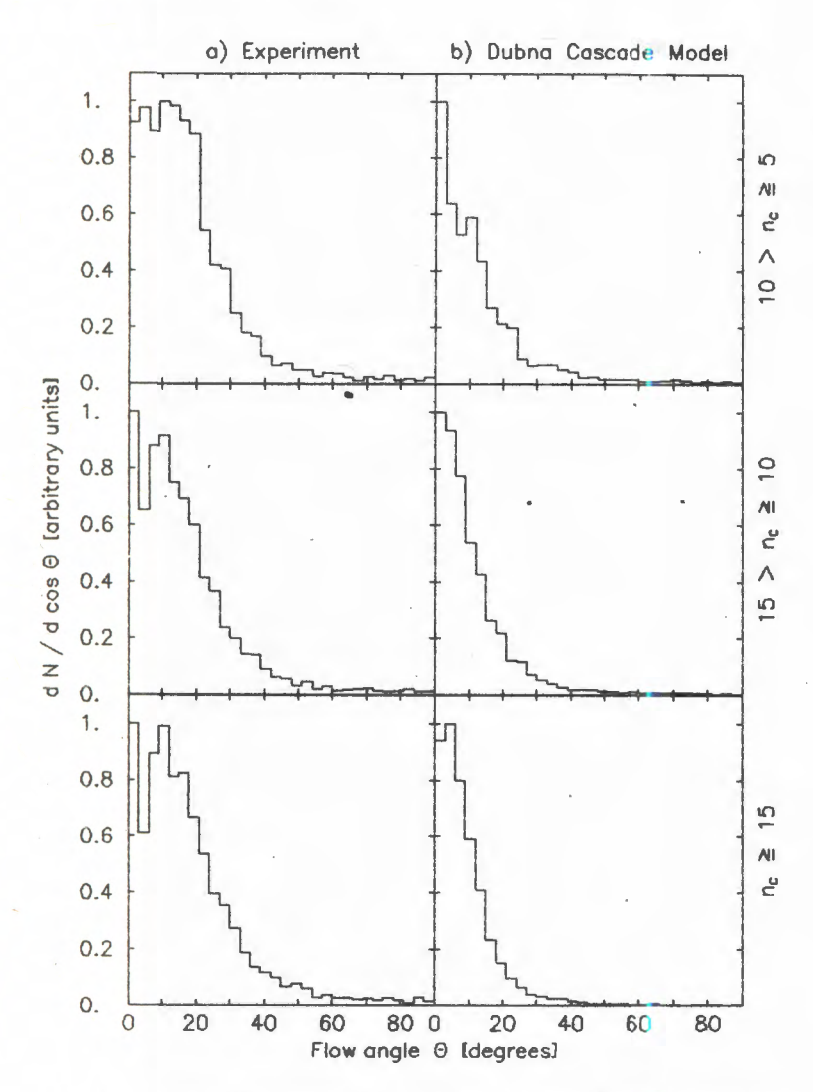


Fig.6. Flow angle distributions for C+C collisions in different multiplicity intervals for participant protons in the c.m.s.

presence of a nonzero peak for the experimental data in the last two intervals of multiplicity while the flow angle distributions for the DCM calculations are peaked at 0°.

Thus, the performed analysis allows us to draw a conclusion that there is experimental evidence of the collective flow of nucleons: the «side-splash» of participants in the collisions of carbon nuclei with tantalum and carbon. It is worth mentioning that in our experiment the flow angle distributions are peaked around 10°—12° for mid- and high multiplicity bins while in the experiments at the BEVALAC energies the finite deflection angle reached considerably larger values. This fact confirms the results obtained earlier at the BEVALAC where for different colliding heavy nuclei the decrease of the «side-splash» effect was observed with increasing energy [14].

#### 4. Conclusion

Results from the global event shape analysis of the C + Ta and C + C data from the 2 m propane bubble chamber are presented. The investigation was made to search for collective motion of nucleons. For this purpose the flow angle distributions were analyzed. We compared the experimental results with the Dubna cascade model calculations. As the collective phenomena are not taken into account by this cascade model, it can serve as a good background for extracting collective effects from the experiment.

From the analysis of the experimental data it was deduced that the collective effect — «side-splash» of participants — is observed and is prominent for C+Ta data in a  $15 < n_c < 35$  multiplicity interval. In C+C this effect is still observable for medium and high multiplicities but less pronounced. It is necessary to note here that the data presented above are the first experimental evidence of the collective effect of this kind in nucleus-nucleus collisions at energy essentially higher than 1 GeV/c per nucleon. The finite deflection angle increases with increasing multiplicity in our experiment as well as at the BEVALAC energies, but this dependence is different for symmetric (C+C) and asymmetric (C+Ta) collisions.

The comparison of the  $\theta_{FL}$  distributions in our experiment with those obtained at the BEVALAC shows that finite deflection angle decreases with increasing energy. This fact is in line with previous experiments at Berkeley. Further investigations of the «side-splash» effect are required to understand the nature of this phenomenon better.

# Acknowledgements

We are very indebted to the team operating the JINR 2 m propane bubble chamber, to the technical staff and to our colleagues at the collaborating institutions for their assistance in film taking and data processing. We are also grateful to H.Lohner for fruitful discussions.

#### References

- 1. Gustafsson H.A. et al. Phys. Rev. Lett., 1984, 52, p.1590.
- 2. Reinfordt R.E. et al. Phys. Rev. Lett., 1984, 53, p.763.
- 3. Doss K.G.R. et al. Phys. Rev. Lett., 1986, 57, p.302.
- 4. Doss K.G.R. et al, Phys. Rev. Lett., 1987, 59, p.2720.
- 5. Gutbrod H.H. et al. Phys. Lett., 1989, 216B, p.185.
- 6. Busza W., Goldhaber A.S. Nucl. Phys., 1984, A419, p.635c.
- 7. Gudima K.K., Toneev V.D. Nucl. Phys., 1984, A400, p.173.
- 8. Armutlijsky D. et al. Yad. Fiz.; 1989, 49, p.182.
- 9. Gasparian A.P., Grigalashvili N.S. JINR, 1-11335, Dubna, 1978.
- 10. Abdrakhmanov E.O. et al. Yad. Fiz., 1978, 27, p.1020.
- 11. Agakishiev H.N. et al. Z. Phys., 1983, C16, p.307.
- 12. Abdrakhmanov E.O. et al. Yad. Fiz., 1978, 28, p.1304.
- 13. Gulassy M., Frankel K.A., Stocker H. Phys. Lett., 1982, 110B, p.185.
- 14. Doss K.G.R. et al. Phys. Rev., 1985, C32, p.116.

УДК 539.1.07

# MC SIMULATION OF ZERO DEGREE CALORIMETER FOR INVESTIGATION OF Pb-Pb INTERACTION AT 160 GeV/NUCLEON IN WA-98 EXPERIMENT

R.Eremeev, A.Fedunov, A.Maximov, G.Shabratova, N.Slavin, A.Vodopianov, V.Genchev\*

The characteristics of the lead Zero Degree Calorimeter have been investigated in the framework of Geant package. This calorimeter is used like the major trigger device of nucleus-nucleus central collisions. The simulation of nuclear interaction of projectile and it's fragments with calorimeter media has been done. The calorimeter resolution as a function of projectile energy is evaluated. The scintillation light absorption in light drivers and the fluctuation of photocathode electrons have been taken into account. The resolution was equal to:

RES = 
$$(49.2 \pm 1)\%\sqrt{E} \oplus (1.89 \pm 0.34)\%$$
.

The maximal radiation load for scintillator tile and light drivers has been estimated. It is equal to 2.31 Mrad for single scintillators tile and 164 krad for single driver at intensity of 10<sup>6</sup> Pb nuclei per spill for 4 runs by 30 days.

The investigation has been performed at the Laboratory of High Energies, JINR.

Моделирование переднего калориметра эксперимента WA-98 по исследованию взаимодействий ядер свинца со свинцом при энергии 160 ГэВ на нуклон

# Р.Еремеев и др.

В рамках моделирующего пакета GEANT исследованы характеристики адронного свинцового калориметра, который используется для выделения центральных ядро-ядерных взаимодействий. Предложен метод моделирования ядерных процессов при прохождении ядра и его фрагментов через вещество калориметра. Оценено разрешение калориметра с учетом поглощения света, испущенного в сцинтилляторе, в световодах, а также флуктуация электронов с катода фотоумножителя. Зависимость разрешения от энергии снаряда может быть представлена в виде

RES =  $(49.2 + 1.0)\%\sqrt{E} \oplus (1.89 + 0.34)\%$ .

<sup>\*</sup>Institute of Nuclear Research and Nuclear Energetics, Sofia, Bulgaria

Найдено, что максимальная радиационная загрузка сцинтилляторов при интенсивности пучка ядер свикца  $10^6$  за сброс в течение 4 сеансов по 30 дней составит 2,31 Мрад, а максимальная загрузка световодов — 164 крад.

Работа выполнена в Лаборатории высоких энергий ОИЯИ.

The interest of a scientific community to an investigation of nucleus-nucleus collisions at high energies was manifested in carring out of copious experiments at high energy nuclear beams in last ten years. The selection of collisions with small impact parameters (central collisions) is an important task in such investigations.

The large acceptance experiment of WA-98 was started in 1994 at CERN SPS. The study of Pb-Pb collisions at 40, 80 and 160 GeV with high statistics of hadrons and photons was planned in it. The Zero Degree Hadronic Calorimeter (ZDC) measured a forward energy flux is used like a major triggering device of central collisions. According to this aim main requirements to the calorimeter are:

- · high resolution of deposited energy measurements;
- · high radiation resistance of the calorimeter.

The MC study of the Zero Degree Calorimeter has been done in the framework of GEANT [1] code. It was carried out in accordance with the above requirements:

- · optimization of ZDC geometry;
- · estimation of the calorimeter resolution;
- estimation of radiation loads for the calorimeter sensitive elements.

# 1. The Calorimeter Geometry

The main purpose of a calorimeter usage in an experiment is a measurement of incoming particle energy, with good resolution. This means that the geometry of calorimeter should provide minimal lateral and longitudinal leakages. There is an additional requirement in the case of a hadron calorimeter. The calorimeter response to hadron and electromagnetic showers should be very close, i.e., compensation should be full. The ZDC geometry has been chosen in accordance with requirements mentioned above. The calorimeter consists of a 35 modules of  $15 \times 15$  cm<sup>2</sup> with a cross section of  $105 \times 75$  cm<sup>2</sup> in the plane perpendicular to the beam direction. It has about 9.4 interaction legth along the beam direction with division of each module into 158 layers of 1 cm lead tile and 0.25 cm polystyrene scintillator tile. Four steel plates have been inserted among these layers for mechanical rigidity of the module. The ratio of the thicknesses of lead and scintillator tiles was chosed to be equal to 4 in order to provide full compensation of the calorimeter [2]. Wave length shifters (WLS) were used like drivers of the scintillator light to photo multipliers.

#### 2. The Calculation Method

The goals of our MC study were to simulate calorimeter features as close to a reality as possible. The detailed consideration is needed, partially, for the description of relativistic nuclei interaction with the calorimeter media and an evaluation of scintillator gamma losses

during it passes through the WLS matter. Before the starting of this consideration we shall discuss some GEANT parameters used in our calculation. First of all, the possible in GEANT frame-work secondary prosses were switch on:

photoelectric effect, pair production, Raleigh effect, positron annihilation, decay in flight, muon-nucleon interaction, compton scattering, bremsstrahlung, δ-ray production, nuclear fission by photon, hadron interaction,

multiple scattering.

The hadron interactions were simulated with the help of the FLUKA package. The values of the energy threshold from which the process of given particle is started have been taken equal to 1 MeV for gamma, electron, hadron, muon and 5 MeV for neutrals. The energy conservation of the primary protons was the main criterion in the choice of these CUT values.

- 2.1. The Interaction of the Fast Nuclei with the ZDC Matter. In our case fast Pb nuclei and their fragments pass through the calorimeter media. They create a huge number of hadrons and fragmentate into nuclei with smaller atomic numbers in the same time. In order to simulate this rather complicated process we combined the following:
  - the GEANT estimation of nucleus ionization losses during it's passage through media;
  - the VENUS [3] calulations of the number and kinematical characteristics of particles, produced in an overlapping area of colliding nuclei;
  - the generation of the projectile nucleus fragmentation characteristics according to the EXPERIMENTal distributions.

The main algorithm was the following:

 the interaction point of a projectile with target nucleus was generated according to the nucleus-nucleus cross section

$$\sigma_{BA}^{\text{inel}} = 71(\sigma_{pA}^{\text{inel}})^{0.29} B^{0.68} \text{(mb)},$$
 (1)

with

$$\sigma_{pA}^{\text{inel}} = 18(\sigma_{pp}^{\text{inel}})^{0.34} A^{0.68} \text{(mb)} ;$$
 (2)

- the degree of projectile fragmentation and it's charge composition were generated according to approximation of experimental distributions for the summary charge of fragments  $(Q = \sum Z_{frag})$  and their charge composition [4] (see Fig.1);
- the perpendicular momentum of the fragment was generated due to parabolic law [5]

$$d\sigma/dP_{\perp} \approx \exp(-P_{\perp}^{2}/2\sigma),$$
 (3)

here

$$\sigma = (1/5)^{1/2} (F(A - F)/(A - 1))^{1/2} P_F, \qquad (4)$$

with the Fermi momentum  $P_F = 221$  MeV/c, A — atomic number of projectile and F — fragment atomic number. There are two simplifications in simulation: the hadron interaction of projectiles and their fragments was switched on only for Pb and Fe targets; the fragment

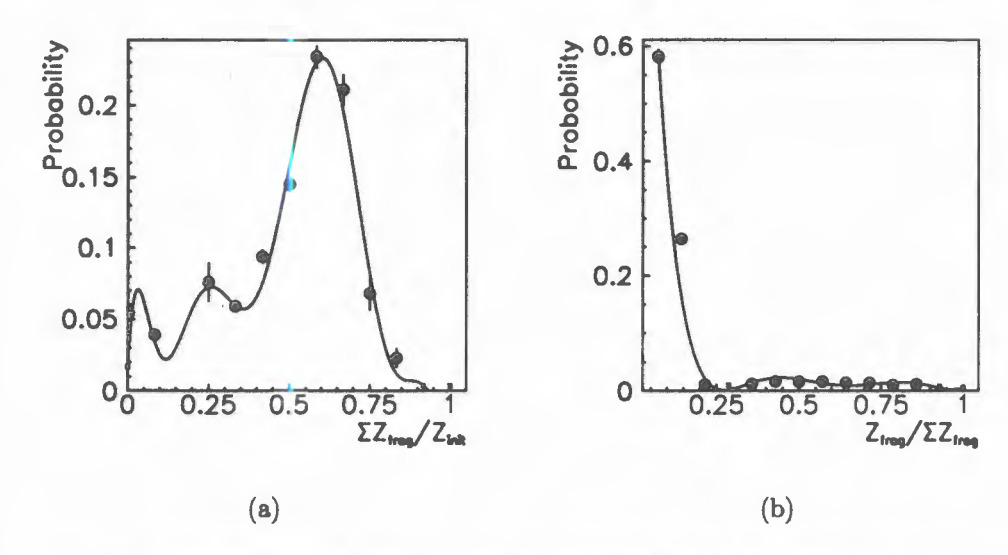


Fig.1. The distributions of: (a) summary charge of fragments and (b) their charge composition

Fig. 2. The scheme of the Pb nuclei fragmentation along it's pass through the ZDC. The values in the square brackets are the numbers of produced particles

with F < 3 were returned to FLUKA as protons with the momentum of 160 GeV/c times their atomic numbers.

One can find in Fig.2 the example of the fragmentation of the Pb nuclei during their pass through the ZDC matter.

2.2. The Attenuation of the Scintillator Light. The losses of the scintillation photons along their light way and the fluctuations of photoelectron have been taken into account.

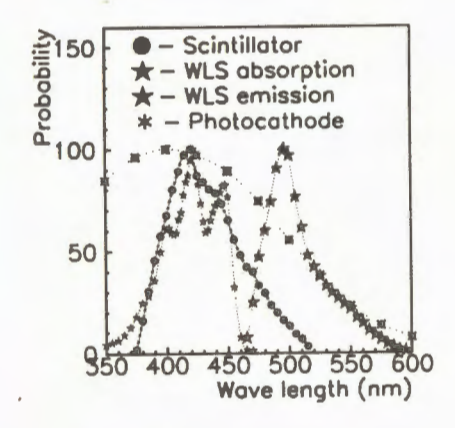


Fig.3. Optical spectra

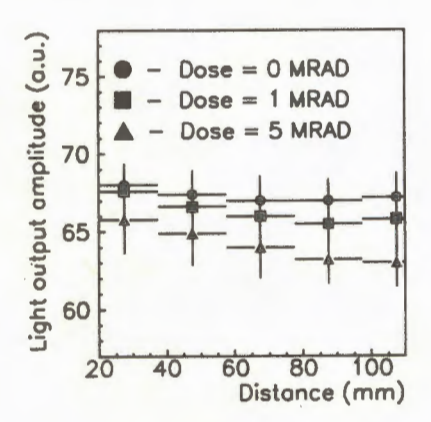


Fig.4. The light output amplitude of scintillator tile as a function of distance from the WLS contact

The number of photons emitted at a given point of a polystyrene tile is equal to:

$$N_{\gamma} = E_{\rm scin} / \varepsilon$$
, (5)

where  $E_{\rm scin}$  is the energy deposited in polystyrene and realised into scintillations,  $\varepsilon = h \langle v \rangle$ — average frequency of emitted light. The spectrum of light emitted by the polystyrene is shown in Fig.3. The influence of the tile transparency to the light collection  $(N_{\gamma}')$  has been done in accordance to the empirical function shown in Fig.4. The scintillator tile was exposed by the radioisotope source and masking then with the black paper. We have used the empirical function for radiation dose equal to 5 Mrad. After this the  $N_{\gamma}'$  has been corrected to the light absorbtion in the wave length shifter medium:

$$N_{\gamma}^{"}=N_{\gamma}^{\prime}\,\mathrm{e}^{-z^{\prime}\,L_{WLS}}\,\eta_{\mathrm{trans}}\,\,,\tag{6}$$

where z is the distance from light creation point to photomultiplier (PM) entrance,  $L_{WLS}$  is the light absorbtion length in WLS and  $\eta_{trans}$  is a transition coefficient including an efficiency of light reemission by the WLS (see Fig.3) and the geometrical efficiency of light transition from the creation point to PM entrance.

A convolution of the spectra of photocathode emission and light emission of WLS—(see Fig.3) has been done in order to take into account the photoelectron fluctuation.

#### 3. Results

3.1. The General Characteristics of the Calorimeter. The geometrical characteristics of the ZDC as a device with almost full deposit of incoming particle energy can be illustrated by the data shown on Fig.5. We see that the huge part of the initial energy is absorbed in

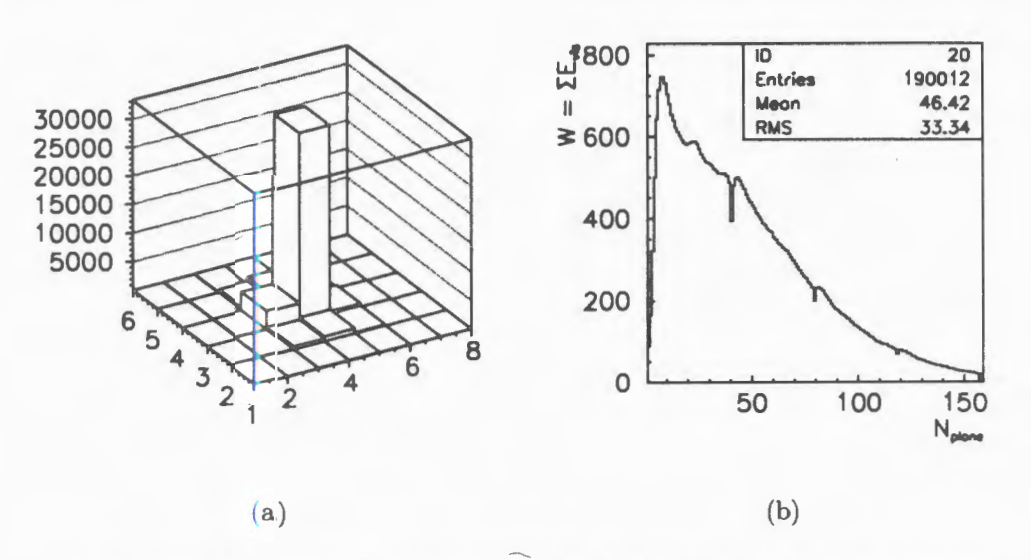


Fig.5. The lateral development of showers initiated by Pb nuclei in ZDC at 160A GeV (a); the longitudinal development of these showers (b)

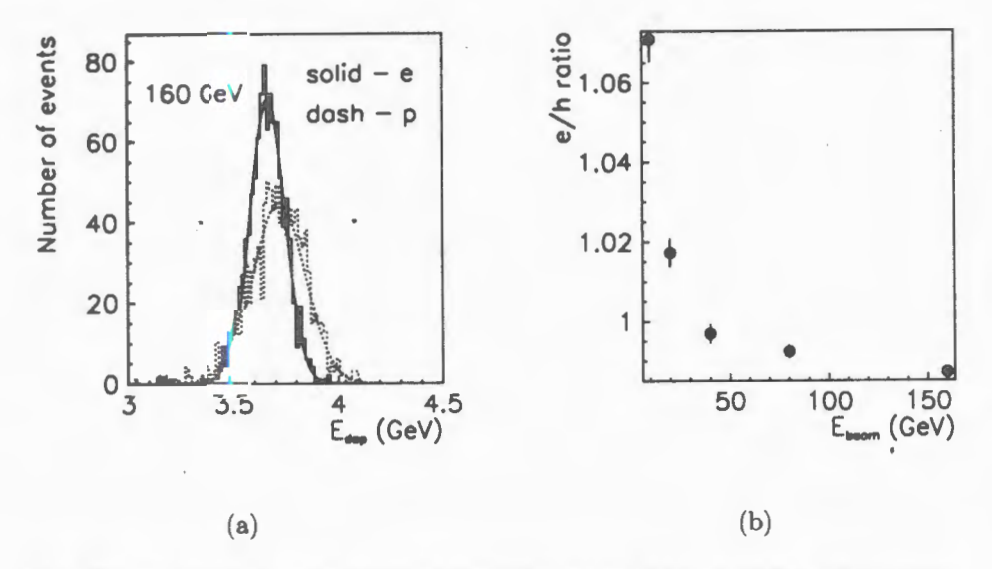


Fig.6. The spectra of the energy deposited in scintillators and WLSs in ZDC at 160 GeV electrons and 160 GeV protons (a); the e/h ratio as a function of initial energy (b)

two central modules of our calorimeter (Fig.5a) both for incoming protons  $(82.505 \pm 0.007)\%$  and for Pb nuclei  $(84.4 \pm 0.7)\%$ . In fact there is no lateral leakage, practically, in our case (Fig.5a). The punchthrough is not larger than 0.6% for the initial proton and 0.4% for the nucleus beam (Fig.5b). The e/h ratios for ZDC are shown in Fig.6.

3.2. The Energy Resolution. The energy resolution of the calorimeter has been estimated for the initial protons. Five beam energies were taken: 10, 20, 40, 80 and 160 GeV. Absorbtion length of the WLS matter varied from 2 up to 10 m. The value of transition coeffisient of  $\eta_{trans}$  from (4) has been taken equal to 0.01 in the semi-emperical way. The results of simulation are shown in the table and Fig.7.

The approximation of the mentioned above resolutions in the form

$$RES = a/\sqrt{E} \oplus b \tag{7}$$

gives the values of coefficients of  $a=(49.2\pm1.0)\%$  and  $b=(1.89\pm0.34)\%$  for  $L_{WLS}=10m$ . The variation of the WLS absorbtion length does not change stochastic term of a, practically. The constant term of b is varied from  $(3.15\pm0.20)\%$  at  $L_{WLS}=5m$  to  $(1.89\pm0.34)\%$  at  $L_{WLS}=10m$ .

Table. Calorimeter resolution at  $L_{WLS} = 10m$ 

$E_{\rm init}$ (GeV)	10	20	. 40	80	160
RES(%)	15.64 ± 0.49	11.78 ± 0.37	7.76 ± 0.20	5.75 ± 0.15	4.38 ± 0.12

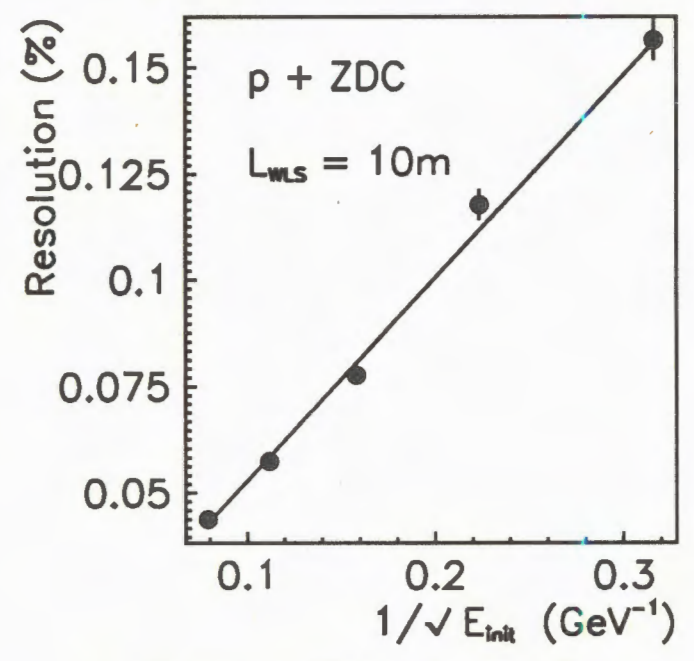


Fig. 7. The resolution of ZDC as a function of  $\sqrt{E_{init}}$ 

Let us estimate an expected accuracy of energy measurement for central collision events (CC) and for minimum bias events (MB), using the energy resolution at  $L_{WLS} = 10m$ . The average values of full energy deposited in scintillation tiles and WLS at 160 GeV/n are:

 $E = 3.784 \pm 0.0002 \text{ GeV}$  for p + ZDC (1000 events),

 $E = 1192.0 \pm 7.0 \text{ GeV}$  for Pb + ZDC (37 events).

Thus the deposited energies will be:

in CC case  $-3.784 \text{ GeV} \times 207 = 783.3 \text{ GeV} \pm 20.2 \text{ GeV}$ ,

in MB case - 1192 GeV ± 28 GeV.

One can see that the selection of central collision events in ZDC can be done with high degree of reliability.

3.3. Radiation Load. The knowledge of the distribution of deposited energy in single scintillator tile and in WLS lets us to estimate radiation load of sensitive parts of our calorimeter in the case of initial Pb nuclei. This value is expected to be rather overestimated as we consider the case when 100% of the beam consist from the Pb nuclei. In the experiment the content of the particles incoming into the ZDC will be spread from Pb nuclei up to single protons. The distributions of the deposited energy for the single tile and single WLS of the central modules as a function of the plane number (longitudinal development of showers) are shown in Fig.8. The areas of maximal energy deposit are hatched. The

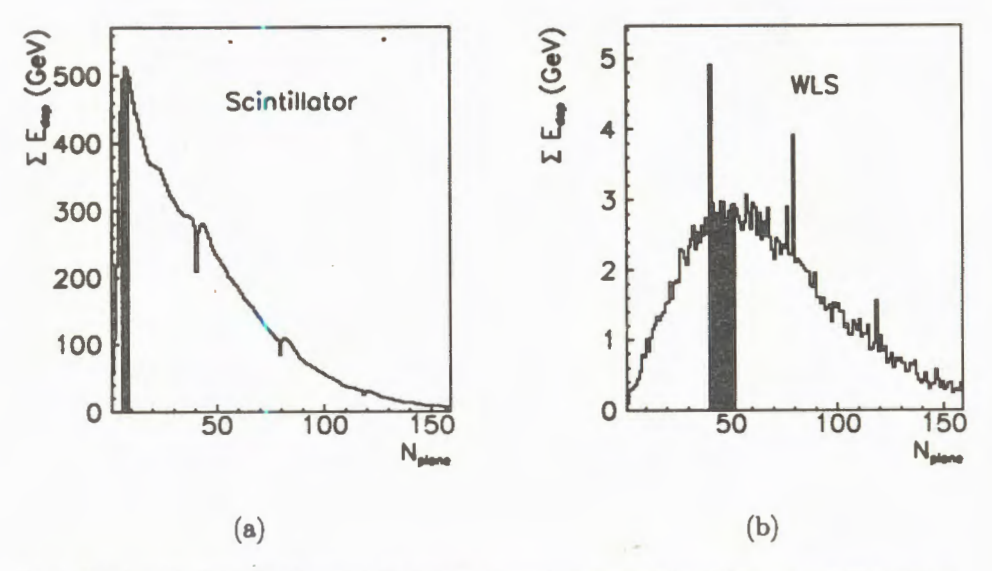


Fig. 8. The longitudinal development of energy deposition in scintillator tile (a) and WLS (b) at 160A GeV Pb nuclei

maximal value for scintillator tile per event is equal to  $13.67~{\rm GeV}$ , for part of WLS with the equivalent volume —  $0.971~{\rm GeV}$ .

The maximal radiation loads suitable to these values for intensity of 10<sup>6</sup> Pb per spill for 4 runs by 30 days are equal to:

for single scintillate plate 2.31 Mrad,

for single WLS 164 krad.

As the radiation load of sensitive parts of ZDC is rather large we have given a trial of an emergency variant to use the lead block in front of the ZDC entrance in order to attenuate the beam intensity. The lead block  $2 \times 2 \times 18$  cm<sup>3</sup> was placed at the entrance of the central ZDC module. The radiation loads were decreased in this case. The scintillator tile, for instance, is loaded up to 1.9 Mrad. The energy resolution is degraded, naturally, and at  $L_{WIS} = 10m$  is equal to:

$$RES = (52.73 \pm 0.49\% / \sqrt{E} \oplus (4.24 \pm 0.29)\%.$$
 (8)

The average deposited energy, in case of MB events, is equal to  $(1053 \pm 48)$  GeV and to  $(782.5 \pm 36.3)$  GeV for CC interactions. One can see that the selection of MB and CC events can be done, in this emergency varuant, with sufficient accuracy, too.

#### 4. Conclusion

- 1. The selection of central collision events can be done with high degree of reliability by means of ZDC measurements.
- 2. The detector parts of ZDC will have a large radiation load during their exposition in Pb nuclei beam. The degradation of ZDC energy resolution as a result of this load can be compensated by the placing of attenuation block in front of ZDC entrance, or by using any semi-peripheral modules like a central.

# 5. Acknowledgments

We are gratefull to B.Batyunya, V.Arefiev and B.Guskov for fruitfull discussions.

#### References

- 1. GEANT, Long Writeup W5013, CERN, Geneva, 1994.
- 2. Wigmans R. NIM, 1987, A259, p.389.
- 3. Werner K. Phys. Lett., 1987, B179, p.225.

- Adamovich M.I. et al. Zeitsch. Phys., 1992, C55, p.235.
   Krasnov S.A., Tolstov K.D., Shabratova G.S. et al. JINR Communication P1-88-252, Dubna, 1988.
- 5. Lepore J.V., Riddel D.J. Report LBL-3086, 1974.

УДК 539.1.07

# AN ALGORITHM FOR IDENTIFYING EVENTS IN THE EXPERIMENT DISTO

M.P.Bussa\*, L.Fava\*, L.Ferrero\*, A.Grasso\*, V.V.Ivanov, I.V.Kisel, E.V.Konotopskaya, G.B.Pontecorvo

An algorithm for identifying useful events in the experiment DISTO is proposed. It is based on the identification of kaons among the secondary charged particles using the measurements of their velocities (with the help of a Cherenkov detector) and deflection algles in the magnetic field. It must be pointed out that within this approach an event can be fully classified by identification of all the detected secondaries.

The investigation has been performed at the Laboratory of Computing Techniques and Automation and Laboratory of Nuclear Problems, JINR within DISTO Collaboration.

# Алгоритм идентификации событий в эксперименте ДИСТО

# М.П.Бусса и др.

Предложен алгоритм идентификации полезных событий в эксперименте ДИСТО. Он основан на выделении среди вторичных заряженных частиц каонов по измерениям их скорости (с помощью черенковского счетчика) и углов отклонения в магнитном поле. В рамках этого подхода возможна четкая классификация регистрируемых событий путем идентификации всех вторичных заряженных частиц.

Работа выполнена в Лаборатории вычислительной техники и автоматизации и Лаборатории ядерных проблем ОИЯИ в рамках коллаборации ДИСТО.

#### Introduction

At present an experiment is being prepared by the DISTO (Dubna — Indiana — Saclay — Torino) [1] collaboration for studying spin effects in the reaction

$$\uparrow pp \rightarrow pK^+Y$$

with the polarized proton beam of Saturne (Saclay, France). The aim is to carry out a detailed study of the reactions  $pp \to pK^+\Lambda^0$ ,  $pp \to pK^+\Sigma^0$  and  $pp \to pp \phi^0$ . For selection of the indicated events (signal events) in the presence of a dominant background, mainly due

<sup>\*</sup>INFN, Torino, Italy

to  $pp \to pp \pi^{\dagger}\pi^{-}$  events, advantage is taken of the fact that signal events are characterized by the presence of a secondary vertex. Earlier, in ref. [2] algorithms for the selection of signal events, based on the identification of secondary vertices, were investigated.

In this paper a new approach to the classification of signal reactions is proposed. Advantage is taken, here, of another feature of the indicated reactions and of the possibility of measuring velocities of detected particles utilizing Cherenkov counters.

### 1. Experiment

The DISTO spectrometer has a cylindrical geometry and consists of two arms situated symmetrically about the beam direction. In each arm there are 5 detectors: 2 scintillation fibre chambers, 2 multiwire proportional chambers (MWPC) and an outer detector, which consists of 2 planes, vertical and horizontal, of scintillation hodoscope counters. At present the possibility of placing Cherenkov counters behind the scintillation hodoscope is investigated. They cover a scattering angle of  $45^{\circ}$  in the horizontal plane and a dip angle of  $\pm 20^{\circ}$ . The detectors and the liquid-hydrogen target are situated in the magnetic field, which is perpendicular to the incident beam.

The layout of the DISTO experiment is presented in Fig.1.

For effective on-line selection of signal events and rejection of back-ground events, a

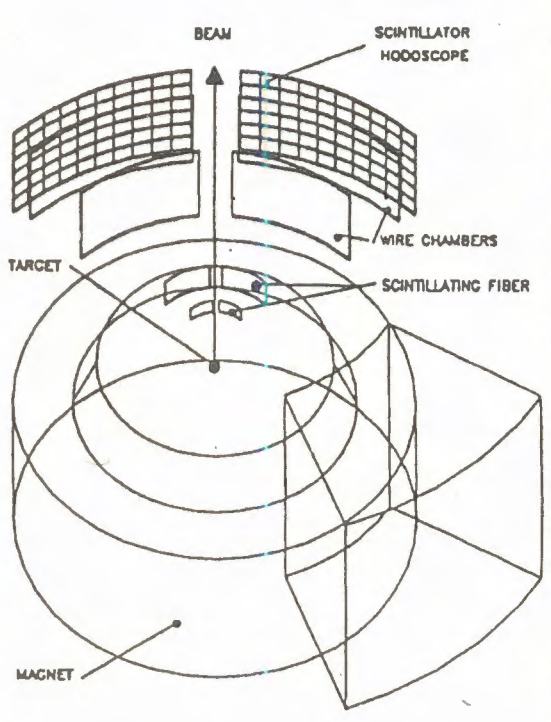


Fig.1. The layout of the DISTO experiment

two-level trigger will be used. The firstlevel trigger is for selection of events by their multiplicity: only four-prong events are selected. For producing the trigger pulse the signals from the scintillation fibre chambers and from the scintillation hodoscopes are used details in the Proceedings [3]). Events accepted by the first-level trigger are examined for the presence of a secondary vertex. At present, two different approaches to searching for the secondary vertex, based on RISC-processors, are under development:

- 1) the dual algorithm [4],
- 2) the method of invariant moment variables together with application of a multilayer perceptron [2].

Utilization in the detecting part of DISTO of Cherenkov counters (see, for instance, Ref. [7]) permitting measurement of the velocities of detected particles opens up a new possibility for the second-level trigger.

### 2. Algorithm for Identifying Secondary Particles

In all the processes of interest there will be charged K-mesons detected in the final state. Therefore, when the selection of events by multiplicities is completed (at the stage of the I-level trigger) and the technique of cellular automata is applied for revealing the curved tracks in the horizontal plane, it will be necessary to identify the detected particles.

To this end we shall first try to reconstruct the momentum of a charged particle by the angle of its deviation in the inhomogeneous magnetic field. The drawing presented in Fig.2 illustrates how the tangent of the deviation angle  $\varphi$  of a charged particle in the magnetic field is determined from the coordinates of «hits» in the fibre chambers (chambers 1 and 2) and in the MWPC chambers (chambers 3 and 4):

$$\tan \varphi = \frac{k_2 - k_1}{1 + k_1 k_2} \,,$$

where

$$k_1 = \frac{x_2 - x_1}{z_2 - z_1} \; ; \qquad k_2 = \frac{x_4 - x_3}{z_4 - z_3} \; .$$

The distribution of random values

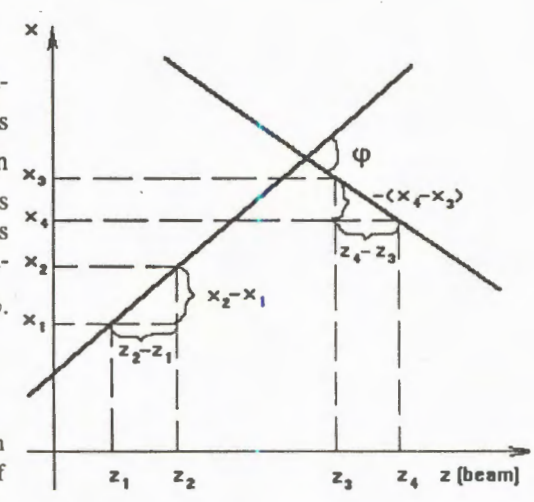
$$C_m = \tan \varphi P$$
,

where P is the momentum of the particle being considered, is presented in Fig.3. From this picture the conclusion can be made that for reconstruction of a great majority of the detected particles  $(p, K^{\pm}, \text{ and } \pi^{\pm})$  one can actually consider the field to be homogeneous, i.e., the particle momenta may be determined from the following relation:

$$P_c = \frac{\overline{C}_m}{\tan \varphi},$$

where  $\overline{C}_m$  is the most probable value of variable  $C_m$ . The distribution of random values  $\Delta P = P - P_c$  characterizing the reconstruction accuracy of momenta for secondary particles with momenta between 0 and 3 GeV/c is given in Fig.4; the distribution of random values  $\frac{\Delta P}{P}$  exhibits a spread amounting to  $\approx 5\%$ .

Fig.2. Deviation angle φ of a charged particle in magnetic field determined by the coordinates of «hits» in the fibre and MWPC chambers



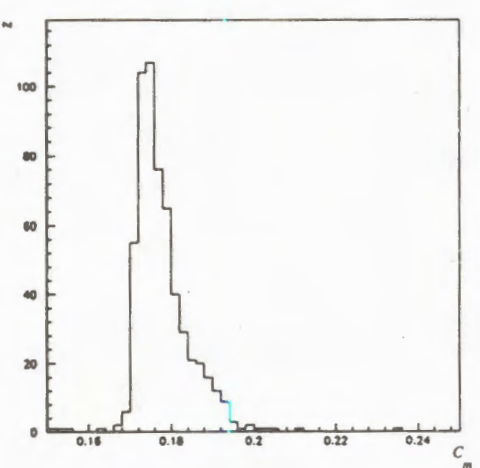


Fig. 3. Distribution of random variable  $C_m = \tan \varphi P$ : P is a charged particle momentum and  $\varphi$  is its deviation angle in the magnetic field

Fig.4. Distribution of random value  $\Delta P = P - P_c$  characterizing the accuracy of momentum reconstruction for secondary particles

Taking advantage of the signal heights from the Cherenkov counter and of the reconstructed momenta of the secondary particles, one can select the events of interest by the presence of  $K^{\pm}$ -meson among the secondaries.

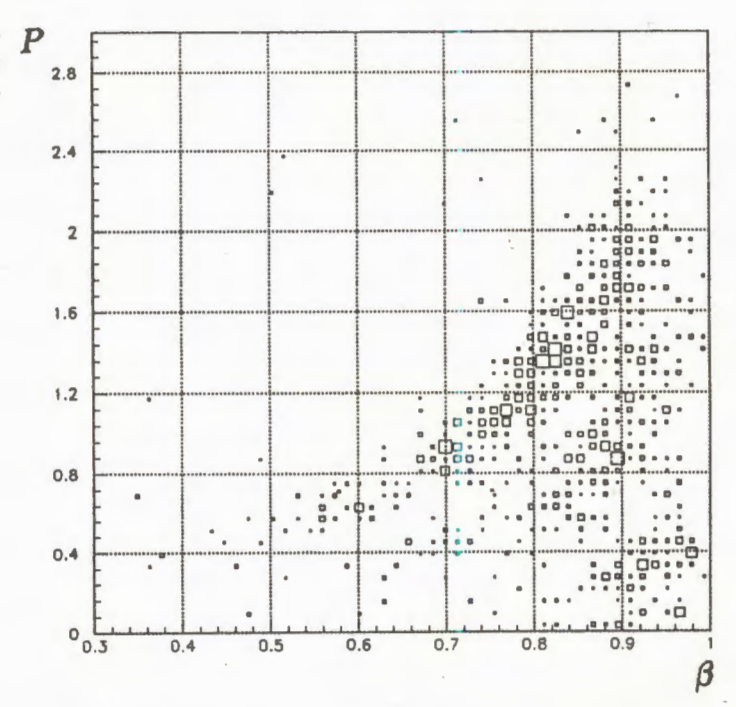
#### 3. Results of Monte-Carlo Simulation

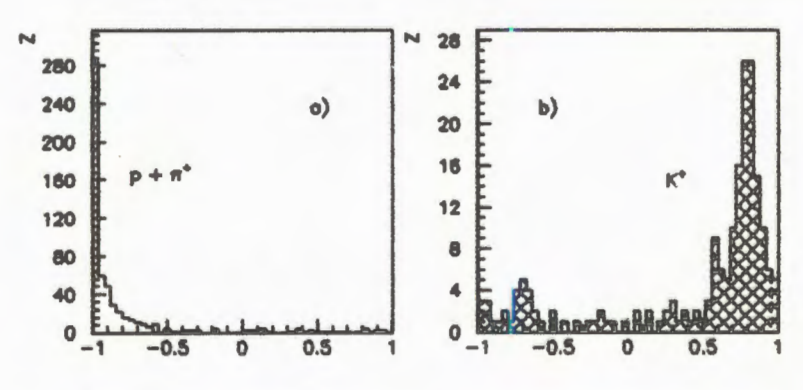
For simulating operation of the experimental apparatus and studying the processes of interest a computer program termed LACYL and based on the GEANT software package [6] has been used. Generation of the primary interaction is done with the aid of the GENBOD code [7], which permits Monte-Carlo simulation of multiparticle events in accordance with the Lorentz invariant Fermi phase space. Each secondary particle (reaction product) is tracked through the known magnetic field, in which it undergoes deflection depending on its charge and momentum, and then through all the detectors taking into account multiple scattering and energy losses occurring in the materials traversed. Unstable particles are allowed to decay in accordance with their lifetimes and branching ratios, and the decay products are also tracked through the apparatus.

In Fig.5. a two-dimensional distribution of the variable «P vs  $\beta$ » is represented. In the example we use the quantity  $\beta = P/E$ , where E is the particle energy. The value of  $\beta$ , obtained from the expression presented above is supplemented with an error equal to  $\Delta\beta$ , generated in accordance with the Gaussian distribution N(0,0.03), which corresponds to an  $\approx 5\%$  error\* for the whole range of  $\beta$  values. From the Figure it can be seen that the secondary p,  $\pi^+$ , and  $K^+$  are quite well separated.

<sup>\*</sup>Estimation reveals that the experimental error should not exceed this value

Fig. 5. Two-dimensional distribution of variables P vs  $\beta$ :  $\beta = P/E$ , where E is the particle energy





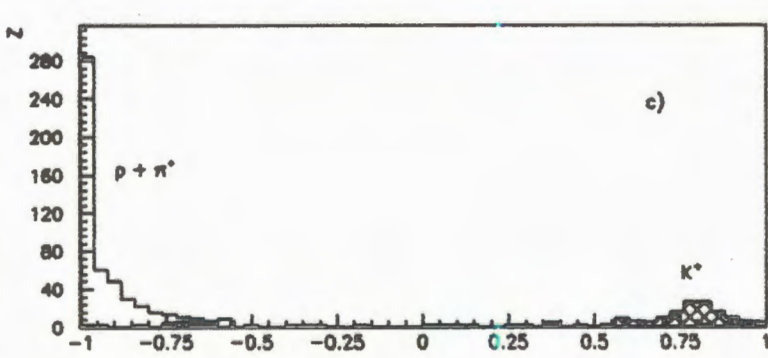


Fig. 6. Distributions of output signals from neural network trained for identification of kaons: a) for tracks of p and  $\pi$ ; b) for tracks of  $K^+$ ; c) summary

As a non-linear classifier permitting identification of the particle under consideration in the space of the indicated random variables one can utilize a multi-layer neural network of the feedforward type from the JETNET 2.0 package [8]. In Fig.6 the distribution is presented of the output signals from a neural network trained, also, for identification of kaons:

• the empty histogram corresponds to tracks of p and  $\pi$ ;

• the dark histogram corresponds to tracks of K<sup>+</sup>.

The probability of identifying kaons amounted to 89%. The efficiency of kaon identification may be increased approximately to the level of 95—97%, if the particle examined is first tested as a proton and then, alternatively, as a pion or a kaon (the order is irrelevant).

#### Conclusion

An algorithm for identifying signal events in the experiment DISTO is proposed. It is based on the recognition of kaons among the secondary charged particles. It must be pointed out that within this approach an event can be fully classified by identification of all the detected secondaries.

#### References

1. DISTO collaboration, Arvieux J. et al. — Proposal 213 at Saturne, 1991.

Ivanov V.V., Pontecorvo G.B. — «An Algorithm for Identifying Secondary Vertices».
 In: Proc. of the Third International Workshop on Software Engineering, Artificial Intelligence and Expert Systems for High Energy and Nuclear Physics, Oberammergau, Oberbayern, Germany, October, 4—8 1993; «New Computing Techniques in Physics Research III», Edited by K.-H.Becks & D.Perret-Gallix, «World Scientific», 1994, p.321—326.

3. «DISTO experiment trigger». DISTO meeting, Torino, September 24, 1992.

- 4. Calligarich E. et al. Nucl. Instr. and Meth. in Phys. Res., 1992, A311, p.151.
- Gill D.R. et al. Experimence No.281 «φ Production and OZI Role». Laboratoire National SATURNE, 29 November 1993.
- Brun R. et al. GEANT3 Reference Manual. CERN Program Library Long Writeup W5013, DD/EE/84-1, 1987.
- James F. «N-Body Event Generator». CERN Program Library Long Writeup W515, 1987.
- 8. Lonnblad L., Peterson C., Rognvaldsson T. «Pattern Recognition in High-Energy Physics with Artificial Neural Networks: JETNET 2.0», Comp. Phys. Commun., 1992, 70, p.167.
- 9. Glazov A., Kisel I. et al. Nucl. Instr. and Meth. in Phys. Res., 1993, A329, p.262.

УДК 539.1.07

# ОПРЕДЕЛЕНИЕ ПРОСТРАНСТВЕННОГО ПОЛОЖЕНИЯ СИГНАЛЬНЫХ НИТЕЙ В ДРЕЙФОВЫХ ТРУБКАХ С ПОМОЩЬЮ ПУЧКА РЕНТГЕНОВСКИХ КВАНТОВ

И.Р.Бойко, Л.С.Вертоградов, В.И.Додонов, В.В.Журавлев, М.А.Йгнатенко, З.В.Крумштейн, М.Ю.Николенко, Г.А.Шелков

Исследованы два метода определения пространственного положения сигнальных проволочек в алюминиевых дрейфовых трубках при сканировании их пучком рентгеновских квантов. Показано, что положение проволочки можно определить с точностью лучше 1 мкм по координате ее тени. Другой метод, основанный на нахождении центра тяжести в зависимости скорости счета самой трубки, работающей в режиме пропорционального счетчика, от координаты положения пучка, также дает высокую точность. При сканировании с шагом 50 мкм получена точность ~ 3 мкм. Существенное улучшение в соотношении сигнал-фон удалось получить путем добавления к углекислому газу 16% О<sub>2</sub>.

Работа выполнена в Лаборатории ядерных проблем ОИЯИ.

# Determination of the Spatial Position of the Sensitive Wires in the Drift Tubes with an X-Rays Beam

# I.R.Boyko et al.

The two methods of finding of the sensitive wires positions in the aluminium drift tubes were tested using an X-rays beam. The wire positions can be determined with precision better than 1  $\mu$ m from its shadow coordinate. Another method based on the determination of the center of gravity in the count rate dependence on the beam position also gives a high precision. With a beam step 50  $\mu$ m the precision of wire position at the level of 3  $\mu$ m was obtained. An essential improving in the signal-to-background ratio was obtained by adding 16% of oxygen to the CO<sub>2</sub>.

The investigation has been performed at the Laboratory of Nuclear Problems, JINR.

#### 1. Введение

Одним из важных вопросов производства модулей дрейфовых трубок для универсального детектора АТЛАС [1] является проверка механической точности установки сигнальных нитей внутри трубок, а также их взаимного расположения внутри модулей. Для этой цели в [2] было предложено сканировать коллимированным пучком рентгеновских квантов мюонные модули и регистрировать с помощью детектора гамма-квантов положение теней от нитей (пассивный метод). Этот метод основан на различной поглощающей способности алюминиевых стенок трубок и вольфрамовых нитей и, как было показано в [3], может обеспечить высокую точность определения пространственного расположения нитей. Однако пассивный метод имеет существенный недостаток. При сканировании модулей больших размеров необходимо контролировать с высокой точностью пространственное положение пучка, которое задается взаимным расположением коллиматоров, находящихся впереди и сзади тестируемого модуля, на протяжении всей длины сканирования, что является достаточно сложной технической задачей.

Другой способ нахождения положения проволочек внутри трубок базируется на различной фотопоглощающей способности проволочки и газа внутри трубки (активный метод). Когда пучок рентгеновских квантов попадает на нить, большое количество рождающихся в нити фотоэлектронов выходит в газовый объем трубки и может быть зарегистрировано, если трубка работает как, например, обычный пропорциональный счетчик. В [4] путем нахождения центра тяжести в зависимости скорости счета трубки от положения пучка рентгеновских квантов удалось восстановить с высокой точностью координаты проволочек в лавсановых трубках, наполненных смесью 70%Xe + 20%CF<sub>4</sub> + 10%CO<sub>2</sub>.

# Активный метод

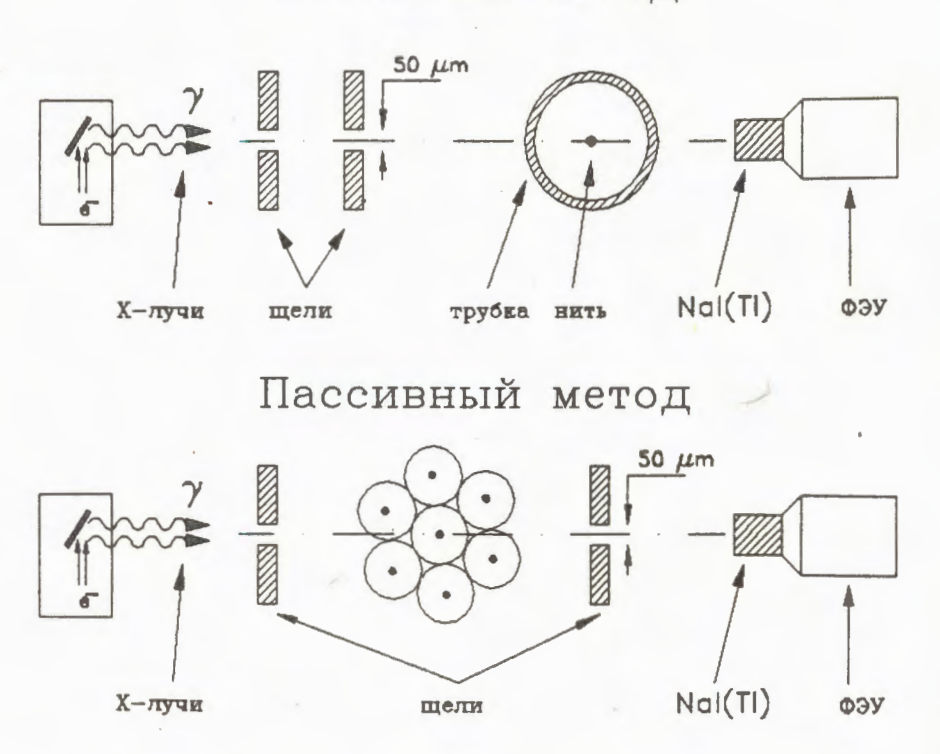


Рис.1. Схема измерения положения проволочек внутри дрейфовых трубок

# 2. Аппаратура

Схема измерений положения проволочек внутри дрейфовых трубок приведена на рис.1. В пассивном методе три слоя алюминиевых трубок с внешним диаметром 3 см и с толщиной стенок 0,5 мм с натянутыми внутри них вольфрамовыми нитями диаметром 50 мкм были помещены между двумя танталовыми коллиматорами, расположенными на расстоянии 20 см. Ширина щелей составляла 50 мкм. Интенсивность прошедшего алюминиевые трубки пучка рентгеновских квантов измерялась с помощью сцинтилляционного счетчика с кристаллом NaJ(Tl) диаметром 15 мм и высотой 30 мм, который размещался непосредственно за вторым коллиматором.

В активном методе пучок рентгеновских квантов также формировался двумя коллиматорами шириной 50 мкм, расположенными на расстоянии 15 см друг от друга. В этом случае определялось положение сигнальной проволочки только в одной трубке. Сцинтилляционный счетчик при этом использовался как монитор интенсивности прошедшего через дрейфовую трубку пучка. Тестируемые трубки работали в пропорциональном режиме. Сигнал с проволочки усиливался токовым усилителем с коэффициентом усиления 70 и подавался на дискриминатор с порогом 7 мВ/50 Ом.

Дрейфовые трубки располагались на подвижной платформе, которая могла перемещаться поперек пучка на расстояние 18 мм с точностью 5 мкм.

В качестве источника рентгеновских квантов использовалась трубка БСВ-21 с вольфрамовым анодом. Размер электронного пятна на аноде этой трубки —  $0.2 \times 8 \text{ мм}^2$ . Рабочее напряжение на рентгеновской трубке было около 20 кВ. На рис.2 представлен энергетический спектр пучка фотонов, прошедшего слой алюминия

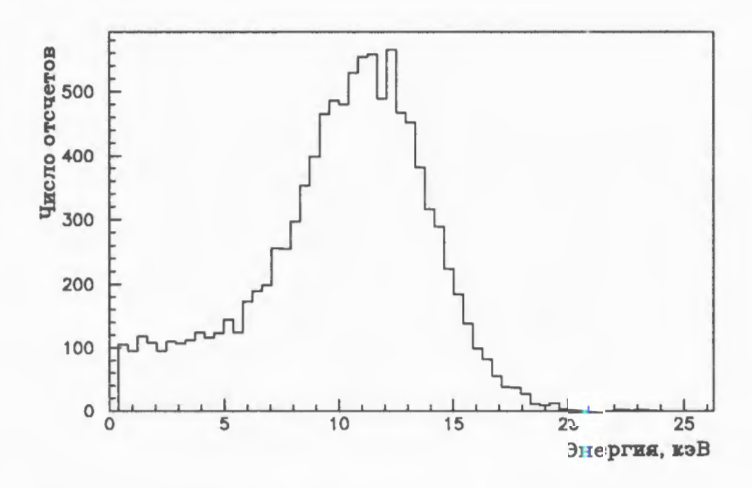


Рис.2. Энергетический спектр рентгеновского пучка после алюминиевого фильтра толщиной 0,5 мм. Напряжение на грентгеновской трубке — 15 кВ.

толщиной 0,5 мм, измеренный с помощью сцинтилляционного счетчика с кристаллом NaJ(Tl), когда напряжение на рентгеновской трубке было 15 кВ. Калибровка амплитуд сигналов со счетчика производилась с помощью набора образцовых гамма-источников, испускающих фотоны в рентгеновском диапазоне. Видно, что основная часть низко-энергетических фотонов поглощалась в аноде самой рентгеновской трубки и алюминиевой стенке исследуемой трубки. Фактически сканирование производилось пучком фотонов с энергетическим разбросом ~ 25%.

## 3. Результаты изиерений

#### а) Пассивный метод

На рис.3 показана скорость счета сцинтилляционного счетчика в зависимости от положения пучка рентичновских фотонов при сканировании с шагом 20 мкм трех слоев дрейфовых трубок. Тени от трех нитей, располагавшихся в различных слоях трубок, отчетливо видны. Точность определения положения тени при данной статистике меньше 1 мкм и определяется точностью шага сканирования. Увеличение ширины щелей коллиматоров приводит к ухудшению соотношения сигнал-фон. Так, для коллиматоров шириной 50 мкм это отношение ~ 10%, а для коллиматоров со щелями 100 мкм оно составляет уже ~ 35%.

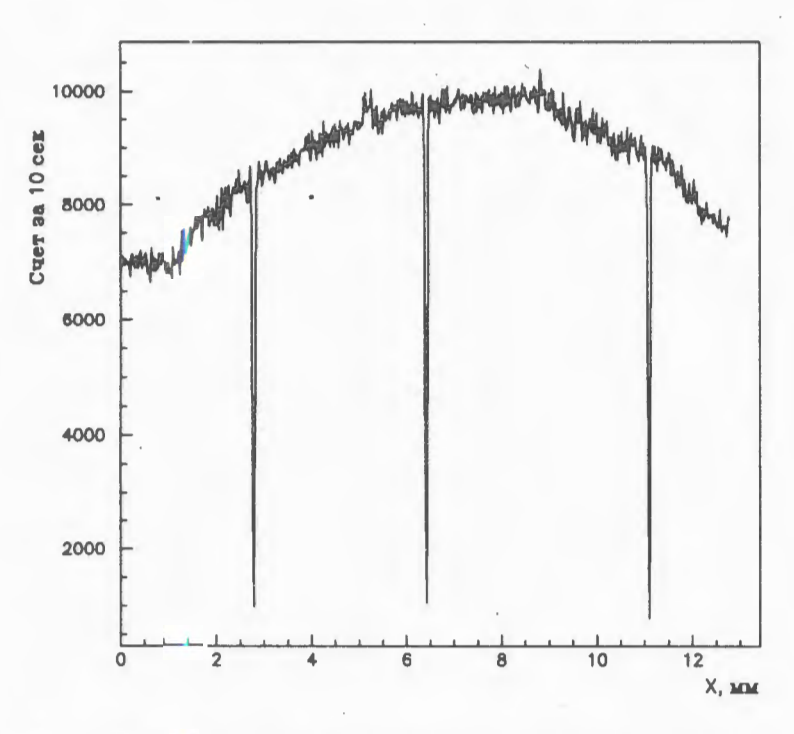


Рис.3. Зависімо сть счета сцинтилляционного счетчика от положения рентгеновского пучка

#### б) Активный метод

Основной задачей выбора рабочих условий в активном методе является усиление отклика трубки на взаимодействие рентгеновского пучка с сигнальной проволочкой и ослабление счета от взаимодействия пучка со стенками и газом трубки. На рис. 4a приведены зависимости скоростей счета монитора и дрейфовой трубки с внутренним диаметром 6 мм и толщиной сигнальной вольфрамовой проволочки 20 мкм, наполненной газовой смесью Ar + 30%  $CO_2$ , от положения рентгеновского пучка. Счет трубки непрерывно возрастал пропорционально количеству газа на пути пучка при приближении к центру. Эффектов от взаимодействия пучка с вольфрамовой нитью или с алюминиевой стенкой не было видно. Это объясняется значительным сечением фото-

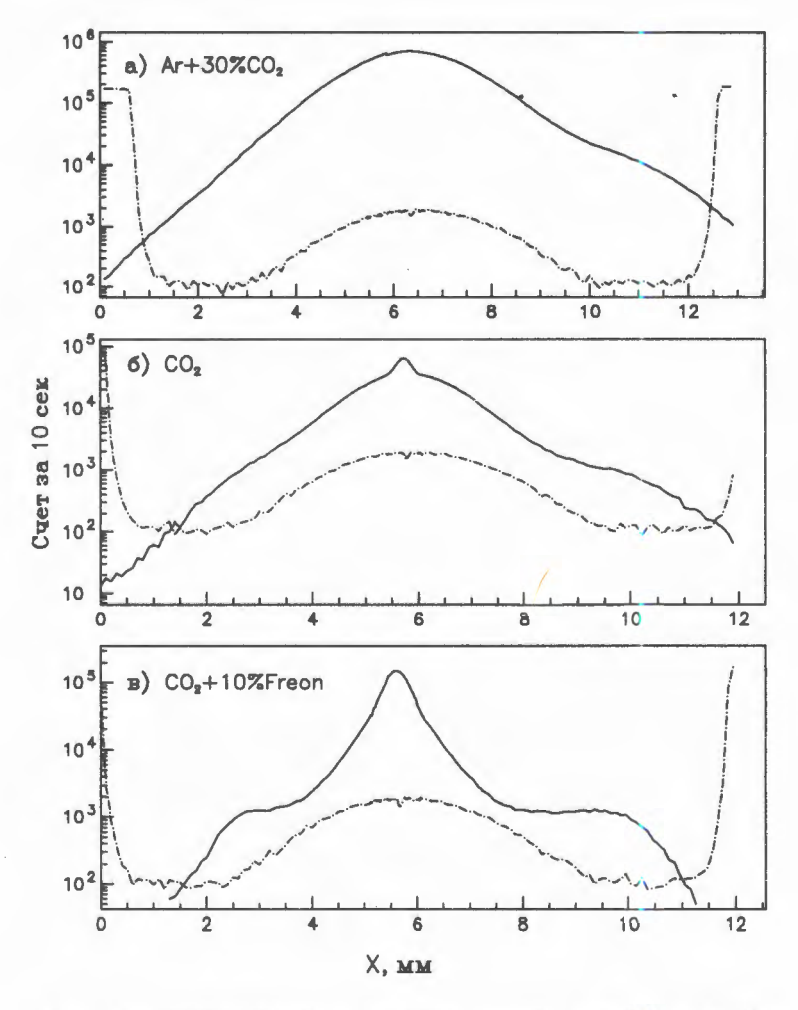


Рис.4. Счет сцинтилляционного счетчика (пунктир) и дрейфовой трубки (сплошная линия) в зависимости от положения рентгеновского пучка

поглощения рентгеновских квантов с энергиями меньше 20 кэВ атомами аргона [5]. Поэтому в дальнейшем использовались только газовые смеси, не содержащие аргона. На рис. 46 приведены результаты измерений при наполнении дрейфовой трубки углекислым газом. Видно, что на фоне широкого максимума, связанного с взаимодействием пучка с газом, отчетливо проявляется пик, вызванный взаимодействием пучка с сигнальной проволочкой.

С целью улучшения соотношения сигнал-фон к углекислому газу было добавлено 10% фреона (13  $\rm B_1$ ). Фреон относится к электроотрицательным газам, которые обладают способностью  $\rm ^{3a}$ хватывать свободные электроны, образующиеся в результате прохождения ионизирующего излучения. Результаты измерений приведены на рис.4 $\rm ^6$ . Добавка к  $\rm CO_2$  10% фреона привела к существенному уменьшению счета трубки, когда пучок проходит вдали от сигнальной нити. Пики, связанные с взаимодействием пучка с газом и нитью, слились в один, ширина которого составила 1,2 мм.

Значительно большим сечением захвата свободных электронов обладает кислород. На рис.5 представлены скорости счета монитора и дрейфовой трубки диаметром 30 мм с вольфрамовой проволокой диаметром 50 мкм в зависимости от положения коллимированного пучка фотонов при наполнении трубки углекислым газом и смесью CO<sub>2</sub> и 16% кислорода. В этих измерениях трубка передвигалась с шагом 0,5 мм, а в области

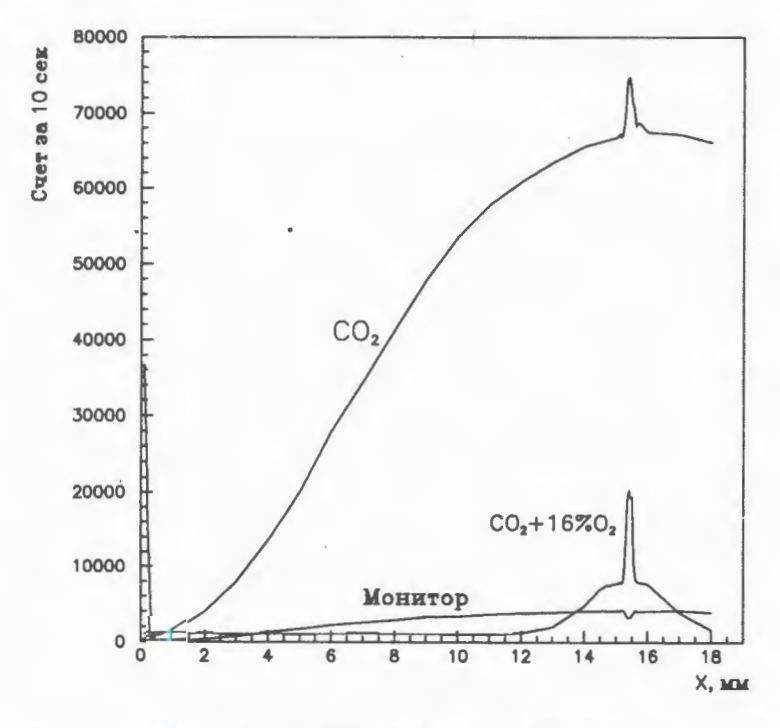


Рис.5. Счет монитора и дрейфовой трубки при наполнении углекислым газом и смесью  ${\rm CO_2}$  + 16%  ${\rm O_2}$  в зависимости от положения рентгеновского пучка

ближе к нити шаг был 50 мкм. Добавление 16% кислорода приводит к почти полной потере эффективности трубкой вдали от анодной нити, и только в области радиусом ~ 2 мм вокруг проволочки заметен эффект взаимодействия фотонов в газе. При этом эффект регистрации фотоэлектронов, образовавшихся на проволочке, отчетливо проявляется на фоне эффекта от взаимодействия в газе. Соотношение сигнал-фон улучшилось более, чем в 15 раз. Фитирование пиков, вызванных взаимодействием пучка с нитью, распределением Гаусса дало ошибку в определении положения центра тяжести ~ 3 мкм. Варьирование концентрации кислорода в смеси с в пределах от 10 до 50% не привело к какому-либо улучшению в соотношении сигнал-фон.

#### 3. Заключение

В заключение сравним преимущества и недостатки обоих методов для X-томографии мюонных модулей. Пассивный метод более прост в реализации сканирования небольших по размеру модулей. Соотношение сигнал-фон в этом методе значительно лучше. Нет необходимости поддерживать системы считывания информации и газового обеспечения. Однако осуществлять контроль положения узкого пучка с точностью несколько микрон на базе нескольких метров — наиболее сложная техническая задача при реализации этого метода. Активный метод сканирования также показал свою эффективность и высокую точность. Он позволяет производить коллимацию рентгеновского пучка более простым способом и, в принципе, не требует перемещения рентгеновского источника (сканирование может осуществляться за счет поворота рентгеновского пучка). Оба исследованных метода могут найти применение для томографии мюонных модулей установки АТЛАС.

# Литература

- ATLAS Technical Proposal for a General-Purpose pp Experiment at the Large Hadron Collider at CERN, CERN/LHC/94-43, LHCC/P2, 15 December 1994.
- 2. Vertogradov L. ATLAS Internal Note, Muon-No-041, May 1994.
- Bonyushkin Yu. et al. Proposal for Tomograph Coordinate Calibration of Drift Tube Packages, EMPACT Internal Note-240, 24 July 1990.
- 4. Fedin O., Mouraviev S., Smirnov A. The First Results of a TRD Cell Prototype Alignment Test with 36 keV X-ray Beam, Atlas Internal Note, INDET-No-057, 1994.
- Baranov S.A. et al. Gamma Sensitivity of Pressurized Drift Tubes, ATLAS Internal Note, Muon-No-036, February, 1994.